UNIVERSITÀ
DI PAVIA

Dipartimento di Biologia e Biotecnologie “L. Spallanzani”

Laurea Magistralis in Neurobiology

Circuit Dynamics of the External Globus Pallidus Following Levodopa Administration: Simultaneous Recordings of Prototypic and Arkypallidal Neurons in 6-OHDA Hemiparkinsonian Mice

Dinamiche dei circuiti del globo pallido esterno dopo somministrazione di levodopa: registrazioni simultanee di neuroni Prototipici e Arkypallidali in topi emiparkinsoniani 6-OHDA

Supervisor:
Antonio Pisani

Experimental thesis by
Chiara Centofanti

Academic Year 2025/2026

ABSTRACT

Parkinson's disease is characterized by the degeneration of nigrostriatal dopaminergic neurons, leading to profound alterations in basal ganglia circuitry and impaired motor control. Recent studies have demonstrated that the external globus pallidus (GPe) is composed of two major neuronal populations, Prototypic and Arkypallidal neurons, which play distinct roles in the regulation of movement. Previous work from the laboratory showed that activation of Arkypallidal neurons suppresses motor behavior and suggested, through calcium imaging experiments, that these neurons become inhibited following levodopa (L-DOPA) administration. However, the electrophysiological mechanisms underlying this effect remained unknown.

The aim of this study was to characterize the electrophysiological responses of Arkypallidal and Prototypic neurons to dopamine replacement therapy using in vivo Neuropixels recordings combined with antidromic optogenetic phototagging in a mouse model of Parkinson's disease. This approach enabled the identification of well-isolated neuronal populations and the characterization of their responses to optogenetic stimulation before and after dopamine replacement therapy.

The results demonstrated that Arkypallidal neurons responded reliably to antidromic optogenetic stimulation under basal conditions and exhibited a marked reduction in firing following L-DOPA administration, providing the first electrophysiological confirmation of previous calcium imaging findings. In contrast, Prototypic neurons showed a significant increase in firing rate after dopamine replacement. The opposite modulation of these two neuronal populations, together with the established inhibitory projections from Prototypic to Arkypallidal neurons, supports the hypothesis that increased Prototypic activity contributes to the suppression of Arkypallidal neurons after dopamine replacement.

Overall, this study provides new electrophysiological evidence supporting a functional interaction between the two principal neuronal populations of the GPe and contributes to a better understanding of the cellular mechanisms underlying basal ganglia function in Parkinson's disease and levodopa-induced dyskinesia.

RIASSUNTO

Il morbo di Parkinson è una patologia neurodegenerativa caratterizzata dalla progressiva degenerazione dei neuroni dopaminergici della sostanza nera pars compacta, con conseguente alterazione dei circuiti dei gangli della base e comparsa di sintomi motori quali bradicinesia, rigidità, tremore a riposo e instabilità posturale. Sebbene il modello classico dei gangli della base si basi sulla distinzione tra via diretta e via indiretta, negli ultimi anni numerosi studi hanno evidenziato una complessità circuitale molto maggiore, mettendo in luce il ruolo di nuove popolazioni neuronali coinvolte nella regolazione del movimento.

Tra queste, particolare interesse ha suscitato il globo pallido esterno (GPe), oggi riconosciuto come una struttura composta principalmente da due sottopopolazioni neuronali funzionalmente distinte: i neuroni Prototipici (Proto), che costituiscono circa il 80% della popolazione del GPe, e i neuroni Arkypallidali (Arky), che rappresentano il restante 20%. Studi precedenti condotti presso il laboratorio hanno dimostrato che l'attivazione dei neuroni Arkypallidali determina una soppressione del comportamento motorio e hanno inoltre suggerito, mediante esperimenti di calcium imaging, che tali neuroni riducono la propria attività in seguito alla somministrazione di levodopa (L-DOPA). Tuttavia, il calcium imaging rappresenta una misura indiretta dell'attività neuronale e non consente di descrivere con precisione le variazioni dell'attività elettrica dei neuroni.

L'obiettivo di questo lavoro è stato quindi quello di caratterizzare, mediante registrazioni elettrofisiologiche *in vivo*, la risposta dei neuroni Arkypallidali e Prototipici alla terapia sostitutiva con L-DOPA in un modello murino di malattia di Parkinson. Particolare attenzione è stata rivolta ai neuroni Arkypallidali, con lo scopo di confermare elettrofisiologicamente la loro inibizione dopo la somministrazione di L-DOPA e di indagare i possibili meccanismi responsabili di tale fenomeno.

Per raggiungere questo obiettivo sono stati utilizzati topi FoxP2-Cre sottoposti a lesione unilaterale con 6-idrossidopamina (6-OHDA), nei quali è stata espressa selettivamente la proteina fotosensibile ChrimsonR o ChETA nei neuroni Arkypallidali mediante vettore virale Cre-dipendente. L'attività neuronale è stata

registrata utilizzando sonde Neuropixels 2.0, che consentono la registrazione simultanea dell'attività di centinaia di neuroni con elevata risoluzione spaziale e temporale. Dopo uno spike sorting automatico mediante Kilosort4 e una successiva fase di manual curation attraverso il software Phy, sono stati selezionati esclusivamente i neuroni ben isolati. Entrambe le popolazioni neuronali sono state classificate sulla base delle loro proprietà elettrofisiologiche; l'identificazione dei neuroni Arkypallidali è stata inoltre validata mediante optotagging antidromico.

I risultati ottenuti hanno dimostrato che i neuroni Arkypallidali rispondono in modo affidabile alla stimolazione optogenetica in condizioni basali e mostrano una marcata riduzione della frequenza di scarica dopo la somministrazione di L-DOPA, fornendo la prima conferma elettrofisiologica delle osservazioni precedentemente ottenute mediante calcium imaging. Al contrario, i neuroni Prototipici hanno mostrato un significativo incremento della propria attività dopo il trattamento dopaminergico. Inoltre, l'analisi delle risposte alle diverse intensità di stimolazione optogenetica ha evidenziato un recupero soltanto limitato dell'attività Arkypallidale dopo L-DOPA. Questi risultati, insieme all'aumento simultaneo dell'attività dei neuroni Prototipici e alle note connessioni inibitorie che questi stabiliscono con i neuroni Arkypallidali, suggeriscono che i Prototipici contribuiscono all'inibizione degli Arkypallidali in seguito alla terapia sostitutiva con L-DOPA.

Nel complesso, questo lavoro amplia le conoscenze sul ruolo funzionale delle due principali popolazioni neuronali del globo pallido esterno e fornisce nuove evidenze elettrofisiologiche sui meccanismi di azione della L-DOPA nella malattia di Parkinson. I risultati costituiscono inoltre una base per futuri studi volti a dimostrare in modo diretto il ruolo causale dei neuroni Prototipici nell'inibizione degli Arkypallidali e a chiarire ulteriormente il contributo di questo circuito alla fisiopatologia della malattia e agli effetti della terapia dopaminergica.

CONTENT

1. INTRODUCTION

1.1 Movement and motor control

Movement is a fundamental characteristic of animal life and enables interaction with the external environment. The generation of voluntary movement requires the coordinated activity of the nervous system and skeletal muscles. Motor commands originate from distributed neural circuits that integrate sensory information, internal goals, and previous experience to produce accurate and adaptive actions. Motor control relies on a hierarchical organization involving multiple brain regions. Cortical areas, including the prefrontal, premotor, and primary motor cortices, contribute to movement planning and execution, while subcortical structures such as the cerebellum and basal ganglia are essential for motor coordination, learning, action selection and the formation of habitual behaviors [1], [2].

Among these regions, the basal ganglia play a central role in the initiation and regulation of voluntary movement, action selection, reinforcement learning, and habit formation. Through extensive reciprocal connections with the cortex and thalamus (Fig. 1), the basal ganglia form cortico-basal ganglia-thalamo-cortical loops that are critical for motor control. The striatum, which serves as the main input nucleus of the basal ganglia, receives excitatory projections from the cortex and thalamus, as well as dopaminergic inputs from the substantia nigra pars compacta. These convergent inputs allow the striatum to integrate motor, cognitive, and motivational information and contribute to the selection and execution of appropriate motor actions [1], enabling the optimization of behavior through experience [2]. The striatum also plays a critical role in procedural learning and habit formation. Evidence from studies on multiple memory systems has demonstrated that the acquisition of motor skills relies heavily on striatal circuits, whereas declarative memory depends primarily on the hippocampal formation [3].

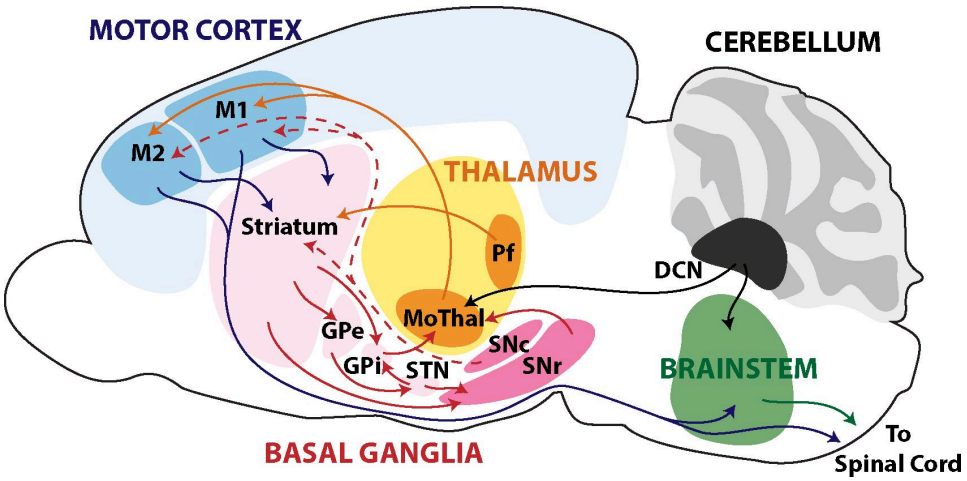

Source: Roth, R. H., & Ding, J. B., Cortico-basal ganglia plasticity in motor learning

Figure 1. *Schematic representation of the principal neural circuits involved in motor control. These include the motor cortex (M1 and M2), the basal ganglia, the thalamus, the cerebellum, and brainstem motor centers. Within the basal ganglia, the striatum serves as the main input nucleus, while the globus pallidus (GPe, GPi), subthalamic nucleus (STN), substantia nigra pars reticulata (SNr), and substantia nigra pars compacta (SNc) contribute to information processing and output. Major anatomical connections between structures are indicated by arrows. MoThal: motor thalamus nuclei; Pf: parafascicular nucleus; DCN: the deep cerebellar nuclei.*

1.2 Basal ganglia organization

The basal ganglia are a group of interconnected subcortical nuclei (Fig. 2) that play a central role in the regulation of movement, as well as contributing to a wide variety of cognitive, motivational, and affective operations.

Rather than simply initiating movement, the basal ganglia are thought to facilitate the execution of desired motor programs while simultaneously suppressing competing or inappropriate motor commands, thereby ensuring the selection of appropriate actions [4].

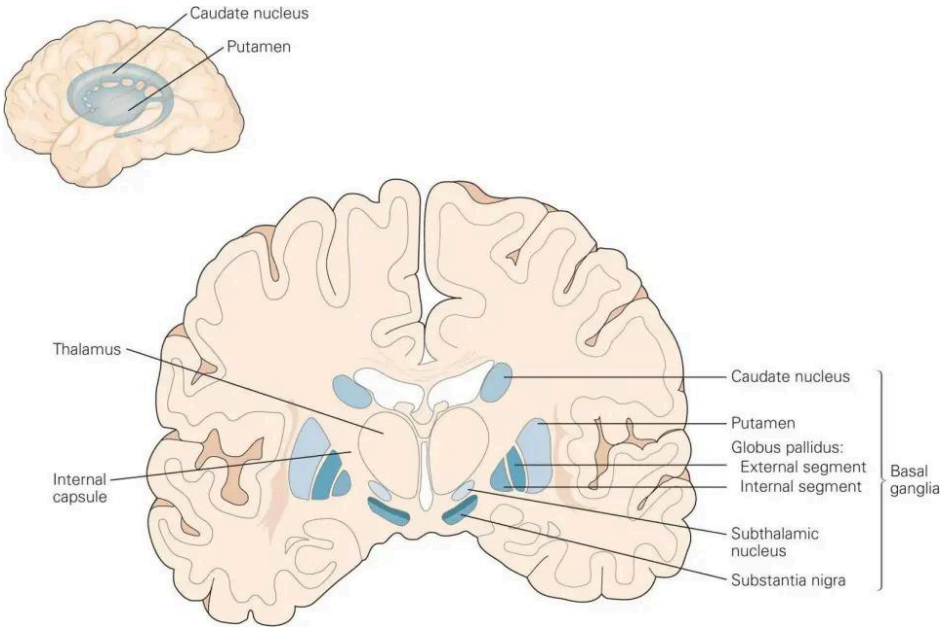

Source: Eric R. Kandel, John D. Koester, Sarah H. Mack, Steven A. Siegelbaum: Principle of Neural Science

Figure 2. *Coronal section of human brain highlighting the nuclei of basal ganglia.*

More than 90% of **striatal neurons** are GABAergic medium spiny neurons (MSNs), so called for their characteristic medium size and abundant dendritic spines, which constitute the principal projection neurons of the basal ganglia. The remaining neuronal population consists of a smaller number of GABAergic and cholinergic interneurons that modulate local striatal processing.

The **subthalamic nucleus (STN)** represents another major input structure of the basal ganglia. In addition to receiving projections from the cortex, thalamus, and brainstem, the STN is unique among basal ganglia nuclei because its neurons are glutamatergic and therefore provide excitatory output. These projections target both the globus pallidus and the basal ganglia output nuclei, contributing to the regulation of motor activity.

Dopaminergic neurons located in the **substantia nigra pars compacta (SNc)** and the **ventral tegmental area (VTA)** constitute an additional modulatory system within the basal ganglia network. Their highly branched axons project widely throughout the brain, with particularly dense innervation of the striatum. By modulating the activity of both projection neurons and interneurons, dopamine plays a critical role in motor control, learning, reward processing, and action selection [5].

Among the output nuclei of the basal ganglia, the globus pallidus is formed by the **external globus pallidus (GPe)** and the **internal globus pallidus (GPi).** Neurons of the GPe receive inhibitory GABAergic inputs from striatal projection neurons and excitatory glutamatergic inputs from the subthalamic nucleus (STN). In turn, GPe neurons, which are predominantly GABAergic, project extensively throughout the basal ganglia network, including to the STN, GPi, substantia nigra pars reticulata (SNr), and striatum itself. The GPi and the **substantia nigra pars reticulata (SNr)** constitute the principal output structures of the basal ganglia. These nuclei are composed mainly of tonically active GABAergic neurons that receive inhibitory inputs from the striatum and excitatory inputs from the STN and they project to motor thalamic nuclei and several brainstem regions [6].

According to the classical model proposed by Roger Albin and colleagues [7], basal ganglia output is determined by the balance between two major pathways. As shown in Figure 3, the **direct pathway**, formed by D1 receptor-expressing striatal neurons projecting directly to the GPi and SNr, facilitates movement by reducing inhibitory output from the basal ganglia. In contrast, the **indirect pathway**, composed of D2 receptor-expressing striatal neurons projecting through the GPe and STN before reaching the output nuclei, suppresses competing motor programs. Dopaminergic input from the substantia nigra pars compacta modulates the activity of both pathways and is therefore essential for normal motor control.

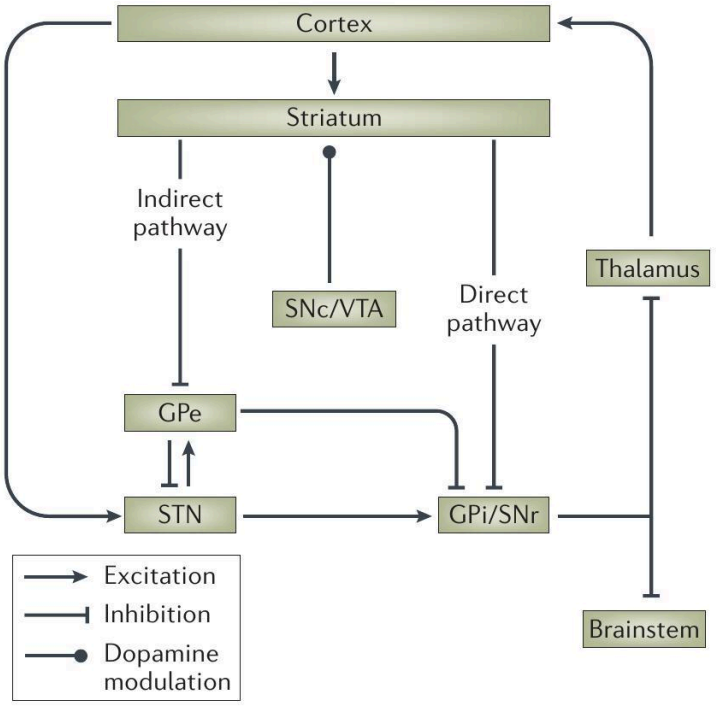

Source: The role of the basal ganglia in habit formation, Henry H. Yin et al.

Figure 3. *Schematic representation of the main connections of basal ganglia. STN, subthalamic nucleus; GPe, external globus pallidus; GPi, internal globus pallidus; SNr, substantia nigra pars reticulata; SNc, substantia nigra pars compacta; VTA, ventral tegmental area*.

The output nuclei of the basal ganglia consist of tonically active GABAergic neurons of high tonic firing rates (40–80 Hz) [8], [9], that exert a continuous inhibitory control over their thalamic and brainstem targets. Modulation of this inhibitory output enables the basal ganglia to regulate the initiation and suppression of behavior.

However, more recent anatomical and physiological studies have revealed that basal ganglia connectivity is much more complex than originally proposed. Additional projections between the striatum, GPe, STN, and output nuclei create highly interconnected networks that cannot be fully explained by the traditional direct–indirect pathway model [5], [10].

1.2.1 Basal ganglia dysfunction and movement disorders

Dopamine plays a particularly important role in regulating basal ganglia activity. Beyond its well-established function in reinforcement learning and motor adaptation, dopaminergic signaling is essential for the normal execution of movement [1].

Consequently, disruption of dopaminergic transmission can profoundly impair basal ganglia function and give rise to severe neurological disorders.

Disorders affecting the basal ganglia commonly manifest as **movement disorders**, which can be broadly classified into three main categories. The first group comprises **hyperkinetic disorders**, characterized by excessive, involuntary movements that interfere with normal motor activity. These abnormal movements are typically reduced by dopamine D2 receptor antagonists and may be aggravated by dopaminergic stimulation. The second group includes **hypokinetic disorders**, such as Parkinson's disease, in which movement is impaired, leading to symptoms such as akinesia, bradykinesia, and rigidity. The third category is represented by **dystonia**, a condition characterized by sustained or intermittent muscle contractions that produce abnormal postures or repetitive movements [7].

1.3 Parkinson's disease

Parkinson's disease (PD) is the most common hypokinetic movement disorder and the second most prevalent neurodegenerative disease after Alzheimer's disease. It affects approximately 1% of individuals over the age of 60, with incidence increasing markedly with advancing age. A small proportion of patients develop symptoms before the age of 50, a condition referred to as young-onset Parkinson's disease. Epidemiological studies indicate that men are affected more frequently than women [11].

- **Clinical phenotype and Motor feature**

Parkinson's disease is characterized by both motor and non-motor manifestations. The age of onset, rate of disease progression and symptoms vary between patients. Several non-motor symptoms may precede the onset of motor signs by years or even

decades. Among the most common prodromal manifestations are hyposmia (reduced sense of smell), rapid eye movement (REM) sleep behavior disorder, constipation, and excessive daytime sleepiness. Motor symptoms typically emerge asymmetrically, often beginning on one side of the body, and gradually worsen over time. The cardinal motor features of PD are bradykinesia, resting tremor and rigidity, which collectively contribute to impaired movement and reduced functional independence [12].

- **Resting tremor** is one of the most recognizable features of PD and occurs in approximately 70–75% of patients [11]. It typically presents as an asymmetric, low-frequency oscillation (3.5–7 Hz) affecting the distal portion of an upper limb, often producing the characteristic "pill-rolling" movement of the fingers. Although tremor may also involve the lower limbs, jaw, or lips, it rarely affects the head or voice [13]. Unlike essential tremor, parkinsonian tremor is most prominent at rest and tends to diminish during voluntary movement or sleep [14].
- **Bradykinesia**, defined as the slowness and progressive reduction in amplitude of voluntary movements, is considered the hallmark motor symptom of PD. It is primarily associated with degeneration of the nigrostriatal dopaminergic system and consequent excessive inhibition of thalamus and cortex, resulting in decreased movement speed [14]. Patients commonly experience difficulty initiating and executing movements, impaired manual dexterity, micrographia, reduced facial expression (hypomimia), decreased blinking, and diminished arm swing during walking [13].
- **Rigidity** refers to an increased resistance to passive movement that is independent of movement velocity [14]. It may affect both proximal and distal muscle groups and is often accompanied by the characteristic "cogwheel" phenomenon when tremor is superimposed on increased muscle tone. Rigidity can contribute to discomfort and pain and may represent one of the earliest manifestations of the disease [13].

- **Etiology**

The etiology of Parkinson's disease (PD) is complex and remains incompletely understood. Current evidence suggests that most cases result from the interaction between **genetic** and **environmental factors**. Although the majority of PD cases are sporadic, genetic causes account for approximately 15% of all cases and are more frequently observed in patients with early-onset disease [15].

Several genes have been identified as contributors to PD pathogenesis. Mutations in SNCA and LRRK2 are typically associated with autosomal dominant forms of the disease, whereas mutations in PRKN, PINK1, and DJ-1 are linked to autosomal recessive inheritance [16].

Environmental exposures have also been associated with an increased risk of developing PD. These include chronic exposure to pesticides and herbicides, rural living, well-water consumption, and contact with industrial solvents such as trichloroethylene (TCE) and perchloroethylene (PCE) [11].

Several pathogenic mechanisms have been proposed to explain the progressive degeneration of dopaminergic neurons. One prominent hypothesis involves **oxidative stress**, where excessive production of reactive oxygen species during dopamine metabolism contributes to neuronal injury [17]. Another major mechanism implicated in PD is the abnormal aggregation of **α-synuclein**, a presynaptic protein that can propagate between neurons in a prion-like manner and constitutes the principal component of **Lewy bodies**, the pathological hallmark of the disease [18].

- **Pathophysiology**

The neuropathological hallmark of Parkinson's disease (PD) is the progressive degeneration of dopaminergic neurons in the **substantia nigra pars compacta (SNc)**, accompanied by the presence of **Lewy bodies**. Neuronal loss is particularly pronounced in the ventrolateral region of the SNc, and it is estimated that approximately 60–80% of nigral dopaminergic neurons are lost before the characteristic motor symptoms become clinically evident. Although Lewy bodies are considered a pathological hallmark of PD, they are not entirely specific to the disease and may be absent in some clinically diagnosed cases [11]. According to the

classical model of basal ganglia dysfunction, the loss of dopaminergic inhibition leads to hyperactivity of indirect pathway striatal neurons, resulting in increased inhibition of the external globus pallidus (GPe). Reduced GPe activity subsequently disinhibits the subthalamic nucleus (STN), increasing excitatory drive to the internal globus pallidus (GPi) and substantia nigra pars reticulata (SNr), ultimately enhancing inhibitory output to the thalamus (Fig. 4) [19].

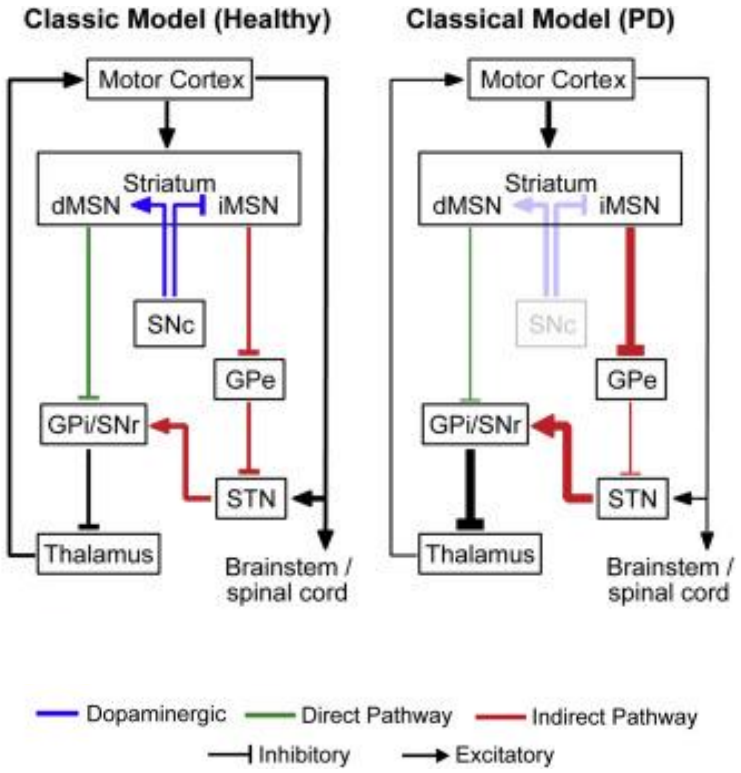

Source: Circuit Mechanisms of Parkinson's Disease, M. McGregor et al.

Figure 4. *Schematic representation of the changes of basal ganglia circuit in Parkinsonism. The left scheme represents the circuits in the "normal" state; the right shows the changes in activity associated with parkinsonism. Blue arrows indicate dopaminergic connections, while red arrows represent the indirect pathway connections and green arrows represent the direct pathway connections. The T-bar arrow indicates inhibitory connections, while the standard pointed arrow indicates excitatory connections. The thickness of the arrows corresponds to their activity. (dMSN: direct Medium Spiny Neurons; iMSN: indirect Medium Spiny Neurons; GPe: external the globus pallidus; GPi: internal globus pallidus; SNc: substantia nigra pars compacta; SNr: substantia nigra pars reticulata; STN: subthalamic nucleus).*

1.3.1 Treatment and levodopa induced dyskinesia

Current treatments for Parkinson's disease are primarily symptomatic and do not stop the underlying neurodegenerative process. Pharmacological therapies aim to restore dopaminergic signaling within the basal ganglia, thereby improving motor function and quality of life. Among these treatments, **levodopa (L-DOPA)** remains the most effective therapy for the management of motor symptoms, particularly for bradykinesia and rigidity. Since its introduction, levodopa has dramatically improved functional outcomes and reduced mortality in patients with PD, although it has not been shown to modify disease progression [11].

L-DOPA is converted into dopamine within the brain, compensating for the loss of dopaminergic neurons in the substantia nigra pars compacta. In the early stages of the disease, dopamine replacement effectively restores motor performance. However, as degeneration progresses, long-term treatment is frequently associated with the development of motor complications, including motor fluctuations and **levodopa-induced dyskinesia (LID)** [20].

LID consists of involuntary, excessive, and abnormal movements that typically emerge during periods of high dopaminergic stimulation. Dyskinesias are generally associated with fluctuations in plasma and brain levodopa concentrations and are thought to result from the intermittent stimulation of striatal dopamine receptors that occurs as nigrostriatal degeneration advances [20]. It results in maladaptive plasticity throughout the basal ganglia network, including alterations in synaptic strength and dendritic spine morphology of both direct- and indirect-pathway spiny projection neurons [18], [19]. Interestingly, dyskinesias do not develop in healthy individuals exposed to levodopa but arise preferentially in PD patients [23]. However, the pathophysiological mechanisms underlying LID are still not completely understood.

According to classical models of basal ganglia function, dyskinetic movements may result from an abnormal reduction in inhibitory output from the basal ganglia output nuclei, particularly the GPi, leading to excessive activation of thalamocortical motor circuits [19].

However, growing evidence suggests that LID involves more complex alterations in basal ganglia activity patterns, including changes in neuronal firing, synchronization, and network connectivity.

In fact, studies reported that the average firing rate of GPe neurons was lower in MPTP-treated monkeys than in normal animals [24].

Understanding these circuit-level mechanisms remains a major challenge and represents an important step toward the development of more effective therapeutic strategies.

1.4 The external globus pallidus (GPe)

The GPe is now considered a major integrative node of the basal ganglia network rather than a passive relay station [19]. More recent studies have demonstrated that it receives convergent input from both indirect-pathway spiny projection neurons (iSPNs) and direct-pathway spiny projection neurons (dSPNs). While iSPNs constitute the predominant source of striatal input to the GPe, dSPNs also send collateral projections to this nucleus, highlighting a more intricate organization of basal ganglia circuits than originally proposed [25], [26], [27], [28].

So, GPe receives inhibitory projections from striatal neurons and excitatory inputs from the STN, while sending widespread inhibitory projections to other basal ganglia nuclei, including the STN, GPi, SNr, and striatum [5].

Alterations in GPe activity represent a prominent feature of the parkinsonian state. Following dopaminergic depletion, GPe neurons exhibit reduced firing rates and increased bursting activity, as observed in both MPTP-treated primates and 6-OHDA rodent models. According to the classical rate model of Parkinson's disease, this reduction in GPe activity results from increased inhibition exerted by hyperactive indirect-pathway striatal neurons. However, alternative hypotheses suggest that dopamine depletion may also impair the intrinsic pacemaking properties of GPe neurons, contributing directly to their abnormal firing patterns [24].

Recent anatomical, molecular, and electrophysiological studies have revealed that the GPe is composed of distinct neuronal populations rather than a homogeneous

group of neurons. Two principal classes have been identified: **Prototypic neurons** and **Arkypallidal neurons**. Prototypic neurons, which constitute approximately 80% of GPe neurons, display fast and regular firing activity and project primarily to downstream basal ganglia nuclei, including the subthalamic nucleus (STN), substantia nigra pars reticulata (SNr), and entopeduncular nucleus (EPN). In contrast, Arkypallidal neurons represent about 20% of the GPe population, exhibit slower and more irregular firing patterns, and project almost exclusively to the striatum (Fig. 5) [29].

The discovery of these neuronal subtypes has significantly revised the understanding of GPe function and suggests that they may play distinct roles in motor control and in the pathophysiology of Parkinson's disease. Indeed, alterations in specific pallidal pathways have been shown to underlie distinct Parkinsonian motor deficits [30], highlighting the importance of understanding the individual contributions of Prototypic and Arkypallidal neurons to basal ganglia function.

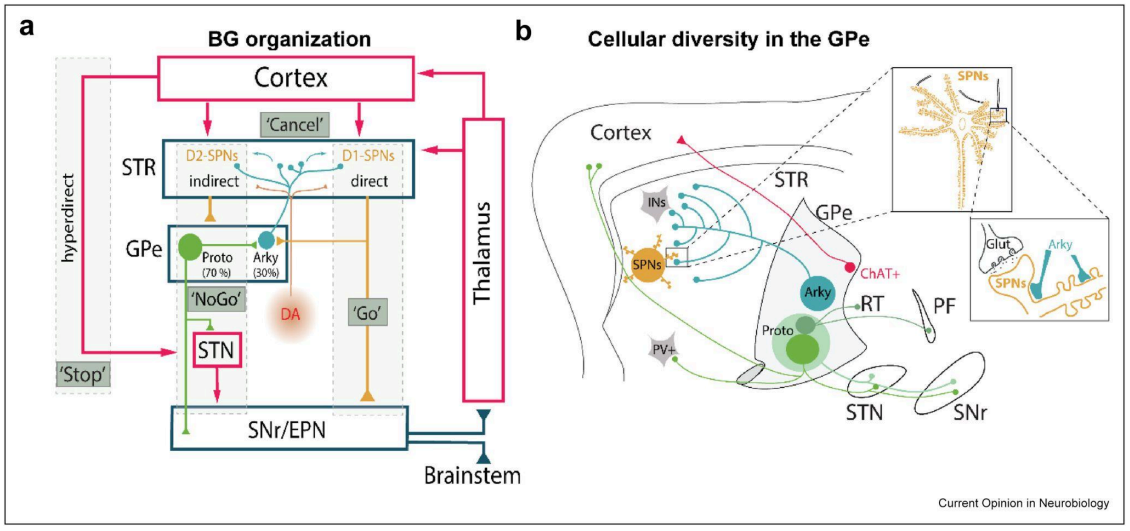

Source: Arkypallidal neurons in basal ganglia circuits: Unveiling novel pallidostriatal loops? - Guilhemsang et al., 2023

Figure 5. *Basal Ganglia organization.* ***a)*** *Schematic representation of the direct/indirect pathways updated with the Prototypic and Arkypallidal neurons.* ***b)*** *Sagittal representation of a rodent's brain, illustrating the main output projections from Prototypic and Arkypallidal neurons. (Arky: Arkypallidal GPe neurons, ChAT+: Choline acetyl transferase expressing neurons of the basal nucleus of Meynert, Glut: Glutamatergic inputs, INs: striatal interneurons, Proto: Prototypic GPe neurons, PF: Parafascicular thalamic nucleus, RT: Reticular thalamus, SPNs: striatal projection neurons).*

1.4.1 New evidence on Arkypallidal neurons

The name of Arkypallidal neurons derives from the Greek word *arkys* ("hunter's net"), reflecting the extensive axonal arborizations they establish within the striatum [29].

Accumulating evidence suggests that Arkypallidal neurons play an important role in movement suppression. Electrophysiological recordings performed during behavioral tasks showed that Arkypallidal neurons are strongly activated by stop signals and increase their firing during successful action cancellation. Their activation is thought to suppress ongoing striatal activity, thereby contributing to the inhibition of planned or ongoing movements [31]. Consistent with this hypothesis, optogenetic activation of Arkypallidal neurons produces a robust reduction in locomotor activity, supporting their role as a neural "stop signal" within basal ganglia circuits [31].

Recent studies have also revealed important interactions between Prototypic and Arkypallidal neurons. Optogenetic and electrophysiological experiments demonstrated that Prototypic neurons exert a strong inhibitory influence on Arkypallidal neurons through local axon collaterals. Activation of Prototypic neurons suppresses Arkypallidal firing, whereas activation of Arkypallidal neurons does not significantly inhibit Prototypic neurons, suggesting the existence of a predominantly unidirectional inhibitory connection from Prototypic to Arkypallidal neurons. This circuit architecture provides a mechanism through which Prototypic neurons can regulate the activity of Arkypallidal neurons and indirectly control striatal processing [32].

The recruitment of Arkypallidal neurons may occur either through direct inputs from D1-expressing striatal projection neurons or indirectly via D2-expressing neurons acting through Prototypic neurons. However, the precise organization of these inputs and their specific contributions to motor control remain incompletely understood [33].

These observations have identified Arkypallidal neurons as a key component of basal ganglia circuits and have generated increasing interest in understanding how their activity is altered in Parkinsonian conditions and following dopaminergic therapies such as L-DOPA.

1.5 From calcium imaging to electrophysiology

Previous calcium imaging studies performed in the laboratory of Mallet et al. suggested that Arkypallidal neurons are inhibited following L-DOPA administration (Fig. 6). Longitudinal imaging revealed a marked reduction in both the amplitude and frequency of calcium transients after dopamine replacement, indicating a substantial decrease in the activity of Arkypallidal neurons across the transition from the Parkinsonian to the dyskinetic state. However, calcium imaging provides an indirect measure of neuronal activity, and a reduction in calcium signal cannot always be unequivocally interpreted as a decrease in neuronal firing. Therefore the electrophysiological correlates of this observed calcium silencing remained unclear.

In addition to directly measuring neuronal firing with millisecond temporal resolution, extracellular electrophysiology enables the simultaneous recording of multiple neuronal populations, providing the opportunity to investigate circuit interactions that cannot be resolved by calcium imaging alone.

Recent studies have proposed several mechanisms that could contribute to the inhibition of Arkypallidal neurons following L-DOPA administration, including increased activity of D1 receptor-expressing striatal neurons [34], modulation through D2 receptor-dependent pathways [35], and inhibitory collateral projections arising from Prototypic neurons. However, how these different circuit elements contribute to the changes in Arkypallidal activity observed *in vivo* remains poorly understood.

The aim of this project was therefore to identify the electrophysiological correlate of the calcium imaging findings and to characterize the temporal dynamics of Prototypic and Arkypallidal neurons following L-DOPA administration. To achieve this, cell-type-specific optogenetic stimulation was combined with Neuropixels multichannel recordings, allowing simultaneous monitoring of large neuronal populations and investigation of the circuit mechanisms underlying Arkypallidal inhibition.

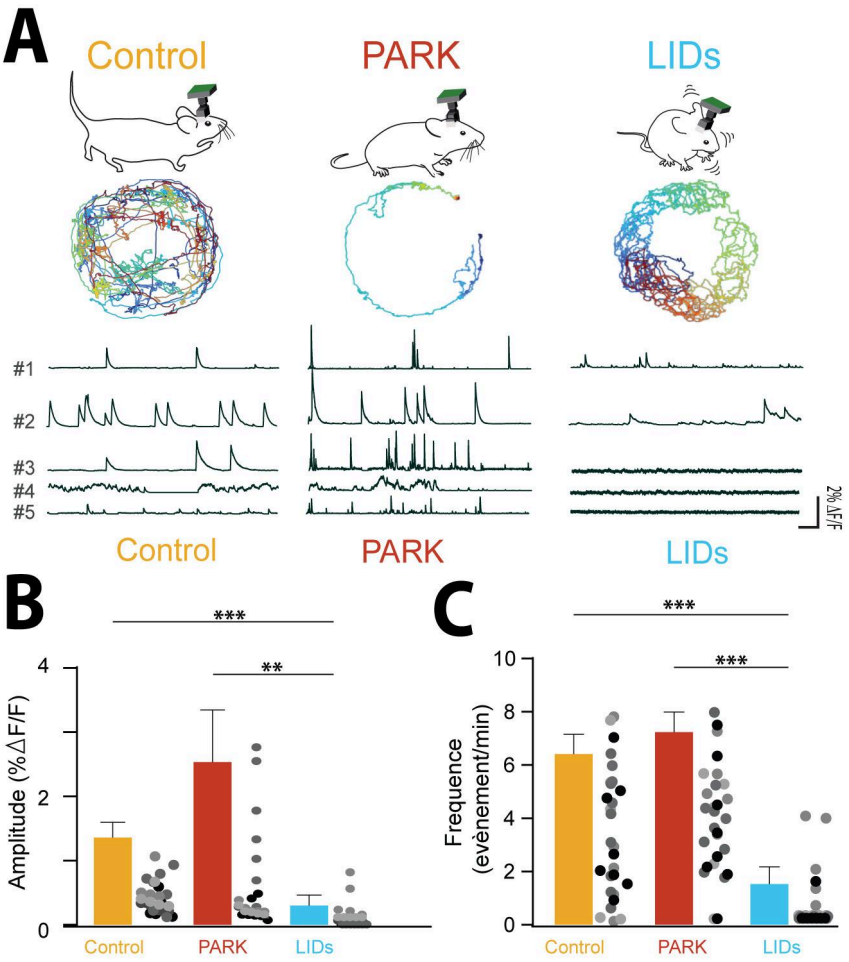

Source: Unpublished data, Mallet et al., IMN Bordeaux

Figure 6. *Longitudinal calcium imaging of Arky-GPe neuron activity across different motor states.* ***A)*** *Schematic of the experimental protocol illustrating longitudinal calcium imaging using a miniscope in control (orange), parkinsonian (red), and dyskinetic (blue) mice. Representative locomotor trajectories recorded under each experimental condition (center) and representative raw calcium traces (bottom) from Arky-GPe neurons across the different motor states. B-C, Amplitude* ***B)*** *and frequency* ***C)*** *of calcium transients for all recorded Arky-GPe neurons (n = 28 neurons from 5 mice).*

1.6 Extracellular recordings: single- vs multi-channel electrode

Traditionally, the understanding of brain function has relied largely on recordings obtained from individual neurons using single electrodes. While these approaches have provided fundamental insights into neuronal physiology, they offer only a limited view of neural circuit activity, as brain functions emerge from the coordinated interactions of large neuronal populations rather than from the activity of isolated cells. To investigate neuronal network dynamics, it is necessary to record simultaneously from many neurons within the same brain region. Achieving this requires both high-density recording devices capable of sampling a large number of neurons with minimal tissue damage and reliable methods for isolating the activity of individual neurons from extracellular signals [36]. The principle underlying these technologies is that neurons located at different positions relative to the recording contacts generate distinct waveform amplitudes across channels. While two neurons may appear indistinguishable on a single electrode, their spatial signatures across multiple recording sites can be used to separate them reliably. This approach also facilitates the identification of overlapping spikes, which may be difficult to resolve using single-channel recordings [37], [38].

Recent advances in multichannel recording technologies have increased the number of neurons that can be monitored simultaneously. Modern high-density probes, such as Neuropixels, contain hundreds of recording sites, enabling the simultaneous recording of activity from hundreds of neurons. These technologies provide an opportunity to study how neuronal populations interact and coordinate their activity to generate behavior [39].

1.6.1 Neuropixel 2.0

Neuropixels 2.0 is a high-density silicon probe designed for large-scale, long-term extracellular recordings. Compared with the original Neuropixels 1.0 design, the probe and the headstage is substantially miniaturized, reducing its size to approximately one-third while maintaining the same number of recording channels (384 channels per probe). This reduced weight makes the system suitable for chronic recordings in freely moving mice.

The probe (Fig. 7) consists of a rigid base containing the electronics required for signal amplification, filtering and digitization, connected through a flexible cable to a miniaturized headstage. The recording shank inserted into the brain is 10 mm long and contains a very high density of recording sites. There are four shanks, and each shank contains 1280 recording sites, resulting in a total of 5120 sites distributed across the probe.

One of the major innovations of Neuropixels 2.0 is its ability to compensate for brain-probe movement during chronic recordings. Because neurons may shift relative to the probe over time, recordings from a given neuron can appear on different recording sites. The dense and highly regular arrangement of recording sites enables computational motion correction, implemented in the Kilosort 2.5 software, an algorithm that estimates tissue movement directly from the recorded spiking activity and realigns the signals across channels [40].

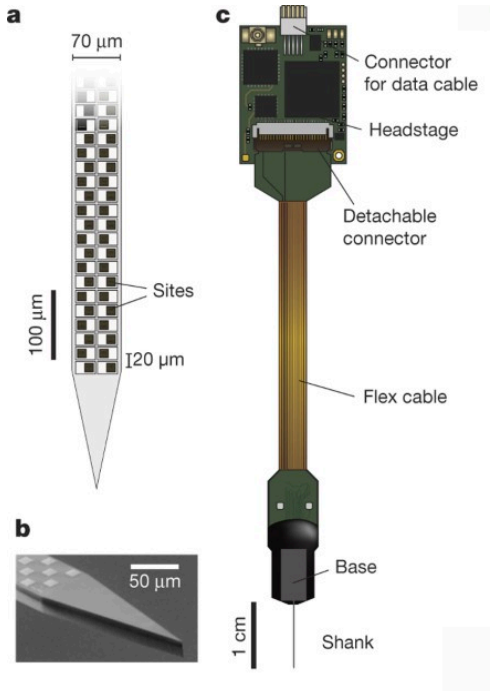

Source: Fully integrated silicon probes for high-density recording of neural activity, James J. Jun et al.

Figure 7. *Representation of Neuropixels 2.0 probe.* ***a)*** *Illustration of probe tip.* ***b)*** *Scanning electron microscope image of probe tip.* ***c)*** *Probe package.*

1.7 Spike sorting

Extracellular electrophysiological recordings measure voltage fluctuations generated by neurons located near a recording electrode. When a neuron fires an action potential, it produces a characteristic voltage deflection, known as a **spike waveform** [41].

The development of high-density recording technologies, such as Neuropixels probes, has enabled the simultaneous recording of large neuronal populations and has driven major advances in data analysis methods. When extracellular recordings contain action potentials from multiple neurons, it is necessary to distinguish neuronal signals from background noise and determine which spikes originate from each individual neuron. This process, known as ***spike sorting***, aims to identify the activity of as many neurons as possible with the highest possible precision, thus grouping the detected spikes into clusters [42]. Many of the spike-sorting approaches developed for single electrodes can be readily adapted to multiple electrodes [38].

Most spike sorting algorithms have the following steps:

1. **Filtering**: low and high pass filter is used to filter the low and high frequency activity, in order to isolate action potentials and visualize the spikes. A compromise should be taken, because on the one hand, one would like to have a narrow filter band to better visualize the spikes, but on the other hand, if the band is too narrow, the filter may hinder different features of the spike shapes.

2. **Spike detection**: from the filtered data, spikes are usually detected using an amplitude threshold. The choice of threshold for detection of a spike event is a compromise between avoiding false positives (i.e., Type I errors) and false negatives (i.e., Type II errors) [43]. A low threshold will capture the most spike events but will erroneously admit many noise events, while a high threshold rejects the most noise but also misses the most spikes. When a statistical model of noise is used, the threshold can be calibrated to a desired ratio of Type I to Type II errors. In most cases, a more permissive threshold is desirable because windows of noise can be removed in later stages of processing. An adequate threshold can be set manually, but an automatic

threshold is preferable, especially when processing a large number of channels [44], [45], [46].

3. **Feature extraction**: the next step is to extract features of the spike shapes.
    - Features can be taken by basic characteristics of the spikes, such as their peak (or peak to peak) amplitude, through amplitude, their width and energy (the square of the signal), their rise slope, fall slope. However, it has been shown that such features are not optimal for differentiating spike shapes in general [7].
    - Another option to calculate spike features is through linear transformations of dataset:
        - A widely used method is Principal Component Analysis (PCA), which represents each spike in a lower-dimensional feature space for subsequent clustering. PCA identifies orthogonal directions (principal components) that capture the maximum variance in the dataset. Each spike waveform is then projected onto these components by computing the dot product between the waveform and the principal component loading vectors, resulting in a set of principal component scores for each spike. In practice, spikes are often represented using the first few principal component scores, which can then be visualized to assess separability between putative neuronal populations. As illustrated in Fig. 8, (a) shows spike waveforms recorded from a single electrode, where two distinct groups of spikes can be visually identified. In (b), PCA transforms the waveform space into a coordinate system defined by directions of maximal variance, and in (c), spikes are represented in this reduced dimensional space using their principal component scores. Clustering is then typically performed in this feature space [38]. However, although PCA identifies the axes with the greatest variance, these axes do not always provide the best discrimination between clusters. Important separation information may lie in components with low variance, which are often discarded.

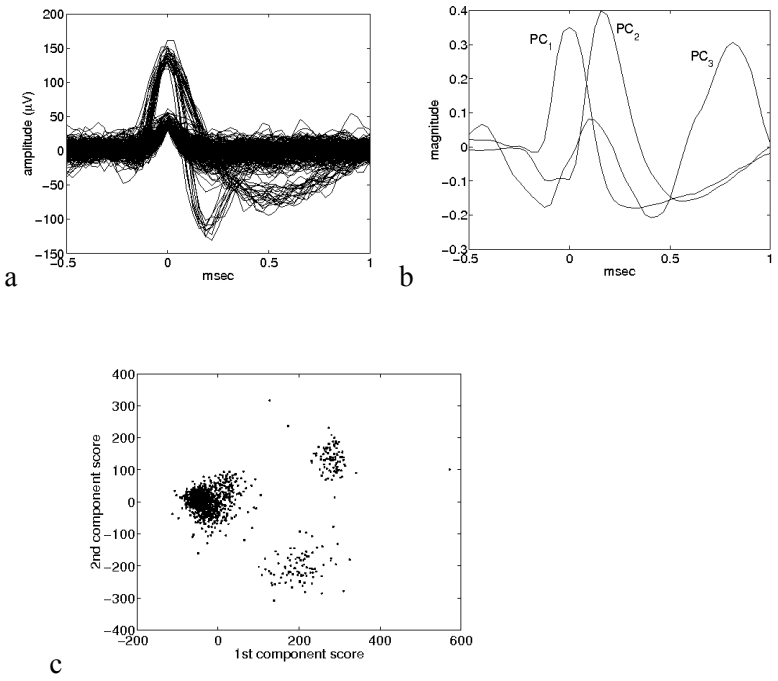

Source: A review of methods for spike sorting - Michael S Lewicki

Figure 8. *Results from principal component analysis of spike data.* ***a)*** *Amplitude of spikes data used in the analysis.* ***b)*** *Representation of the first three principal components.* ***c)*** *Scatter plot of the scores corresponding to the first two principal components.*

- A superior performance is given by the use of wavelet transform [47], a method based on the quantification of energy found in specific frequency bands at specific time locations during each spike profile. To obtain this localized time–frequency information, a discrete wavelet analysis upon the temporal profile of each detected spike is performed.

4. **Clustering**: the final step is to group spikes with similar features into clusters, corresponding to different neurons. Clustering can be done manually or automatically. The manual clustering, however, can be very time-consuming and can introduce errors due to overlapping clouds in cluster space and to the similarity of clusters corresponding to different cells and due to human biases [36]. A more advanced solution is to use automatic clustering, like K-Means, Fuzzy C-Means, Hierarchical, SPC, Gaussian Mixture Models and so on [6].

1.7.1 Kilosort4

One of the algorithms used for spike sorting of Neuropixels recordings is Kilosort. In this study, Kilosort4 was employed. As said, the traditional approach to spike sorting is to divide the process in different steps; **Kilosort4** instead integrates these processes within a **template deconvolution** framework. It first detects candidate spikes using a set of generic templates spanning different waveform shapes and spatial positions. Principal component (PC) features are then computed from these detected spikes and used for an initial graph-based clustering. The average waveform of each resulting cluster forms a **learned template**, representing the characteristic spatiotemporal extracellular waveform of a neuron. These templates are subsequently matched to the recorded signal and iteratively subtracted from it, allowing the detection of overlapping spikes . Unlike previous versions of Kilosort, the learned templates are not used as the final neuronal clusters but are discarded after spike extraction, allowing the final clustering to be performed on the deconvolved spike features.

The deconvolved spike features are subsequently grouped into neuronal units using a **graph-based clustering** algorithm. Instead of directly assigning spikes to clusters using methods like k-means, the algorithm first represents each spike as a point in feature space, where nearby points correspond to spikes with similar waveform characteristics. A graph is then created by connecting each spike to its nearest neighbours, and modularity optimization is applied to identify groups of spikes that are more strongly connected to each other than to the rest of the graph. These groups form the initial clusters, each ideally corresponding to one neuron.

These clusters are subsequently refined using a **merging tree strategy**. Candidate clusters are evaluated to determine whether they originate from the same neuron based on criteria including **refractory period violations** and **projection bimodality**. If merging two clusters produces numerous refractory period violations, the merge is rejected because a single neuron cannot generate spikes within its refractory period. Similarly, waveform projections are examined to determine whether they form a unimodal distribution, suggesting a single neuron, or a bimodal distribution, indicating two distinct neuronal populations [48].

1.7.2 Problems in spike sorting

After spike sorting, errors and misclassifications may still occur. Therefore, the quality of the sorted units must be assessed through a curation process combined with the evaluation of quality metrics. Different metrics can be used to evaluate unit quality and determine whether a cluster represents a well-isolated neuron.

- **Noise**. Noise and recording artifacts may arise from several sources, including movement of the recording probe due to brain motion, mechanical instability, electrical interference, or behavioral events such as licking, which can contaminate extracellular signals and compromise spike sorting. Therefore, careful manual curation is essential to avoid incorrect unit classification. One useful criterion for identifying well-isolated single units is the spatial decay of spike amplitude across recording sites. Because Neuropixels electrodes are closely spaced, the extracellular action potential generated by a single neuron is detected simultaneously on multiple neighboring channels, with the largest amplitude observed on the electrode closest to the neuron and progressively smaller amplitudes on more distant sites. In contrast, electrical noise or artifacts generally do not exhibit this characteristic spatial profile [40], [49], [50].
- **False positives**. occur when spikes generated by two or more neurons are incorrectly assigned to the same cluster. This is more likely to occur when neurons are located far from the recording sites, resulting in low-amplitude waveforms that are difficult to distinguish from neighboring units, or when substantial relative motion between the brain tissue and the probe causes waveform drift throughout the recording. One of the principal methods used to identify false-positive units is the inspection of the **inter-spike interval (ISI) distribution** (Fig. 9A), which plots the time interval between consecutive spikes within a cluster. The x-axis represents the inter-spike interval (ms), whereas the y-axis indicates the number of intervals. Because a single neuron cannot generate two action potentials within its absolute refractory period (typically 1–2 ms), the presence of numerous spikes within this interval suggests contamination by spikes from another neuron [40], [49], [50]. A complementary visualization is the **autocorrelogram (ACG)**, which represents the temporal relationship between all pairs of spikes

belonging to the same unit [51]. The x-axis corresponds to the time lag (ms) between spike pairs, while the y-axis indicates the number of spike pairs observed at each lag. Well-isolated neurons typically exhibit a clear reduction in counts around 0 ms, reflecting the refractory period. However, the absence of refractory period violations alone does not guarantee that a cluster corresponds to a single neuron, since spikes from two neurons firing at different times may still be merged without producing violations. For this reason, additional quality metrics are required. One useful approach is to examine the **amplitude scaling factor as a function of time** (Fig. 9B), in which each point represents an individual spike. A progressive or abrupt change in spike amplitude over the course of the recording may indicate electrode drift or the erroneous merging of spikes originating from different neurons [47], [48].

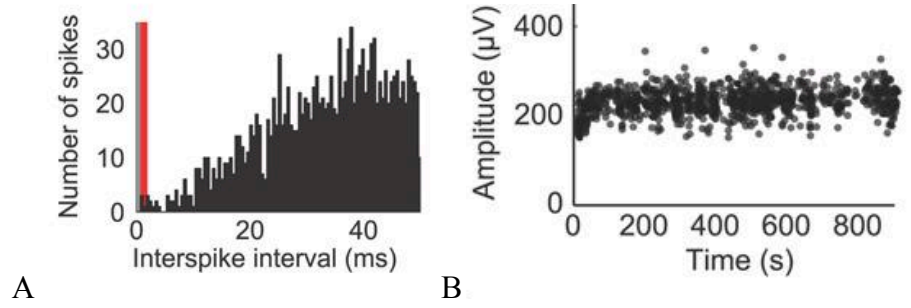

Source: Quality metrics to accompany spike sorting of extracellular signals - Daniel N Hill

Figure 9. ***A)*** *Interspike interval (ISI) histogram that shows a low amount or lack of spike events during the refractory period (red line); bin width is 0.25 ms.* ***B)*** *waveform amplitude as a function of time; bin width is 10 s.*

- **False negatives**. occur when spikes of a neuron are split in different units or some other spikes are not detected at all. This can occur in bursty cells, drifts, artifact masking or when spikes are present below the threshold for detection. It's possible to recognize the number of spikes whose waveforms are **below the threshold** by using the histogram of the values of the spike detection metric (Fig. 10). In particular, the histogram of spike amplitudes can be used to infer the presence of sub-threshold events that are not captured by the

detection algorithm. By modeling the distribution of detected spike amplitudes, it is possible to estimate the fraction of events that fall below the detection threshold and are therefore likely to have been missed [12].

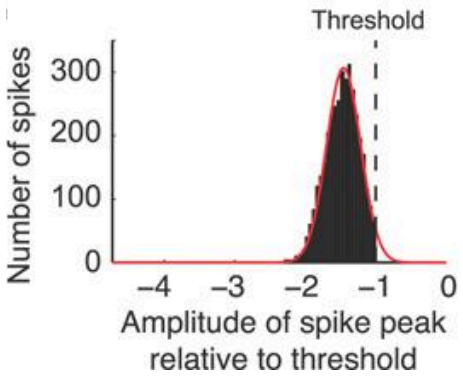

Source: Quality metrics to accompany spike sorting of extracellular signals - Daniel N Hill

Figure 10. *Histogram showing the distribution of spike waveform amplitudes relative to the threshold used for detection. The red curve represents a Gaussian distribution used to estimate the number of spikes from the neurons that were not detected because their amplitudes fell below threshold.*

In the case of **bursty cells** that generate fast sequences of action potential, the amplitude changes across the burst (Fig. 11A) and they might be assigned to different clusters. Evidence of such erroneous splitting can be identified by examining the interspike interval (ISI) distribution. When spikes from the same bursting neuron are divided into multiple clusters, characteristic peaks may appear at short intervals corresponding to the intraburst firing pattern. Similarly, the cross-correlogram (Fig. 11B) computed between the separated clusters often shows a prominent peak at very short latencies (typically around 2–3 ms), indicating that the clusters are not independent neurons but rather originate from the same bursting cell. These observations suggest that the clusters should be merged during manual curation [52].

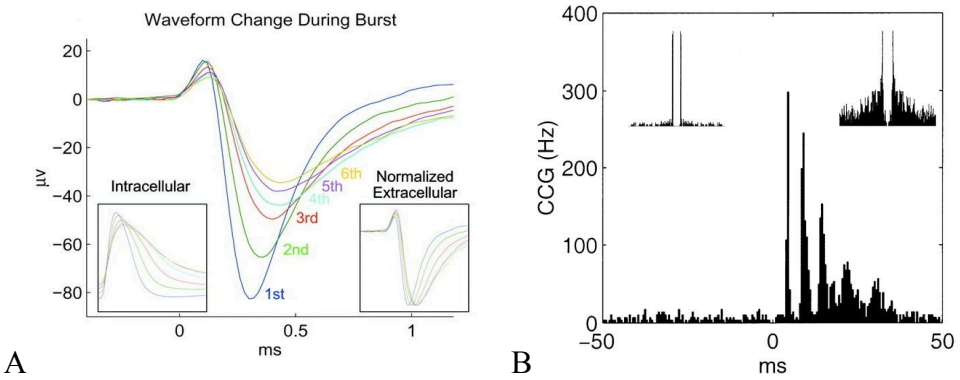

Source: Accuracy of Tetrode Spike Separation as Determined by Simultaneous Intracellular and Extracellular Measurements - Kenneth D. Harris

Figure 11. ***A)*** *Representation of a clear amplitude decrease of the mean waveforms for 6 spikes of a burst. The left square is the corresponding mean intracellular waveforms, while the right panel is the extracellular waveforms normalized by amplitude, showing wave shape change during burst.* ***B)*** *Cross-correlogram of a bursty cell, showing large asymmetric peaks, which indicates that 2 clusters both contain spikes from a single bursting cell.*

Another cause of false negatives could be the **electrode drift**. Over the course of a recording, small movements of the brain tissue relative to the electrode can alter the position of neurons with respect to the recording sites. Consequently, the waveform amplitude and shape of a neuron's spikes may gradually change over time, leading spike-sorting algorithms to incorrectly split the activity of a single neuron into multiple clusters [52].

To identify and correct these errors, several quality metrics are routinely evaluated during cluster curation.

1.7.3 Curation of spike clusters

Following automated spike sorting, a final curation step is required to verify and refine cluster assignments. Although modern spike-sorting algorithms provide great consistency and low error rates, automated clustering is not always sufficient to accurately isolate individual neurons, as shown previously. Curation can be done manually, using algorithms like **Phy** (explained in detail in the 'methods' section) or can be automatic, by using programs like SpikeInterface, Bombcell and others.

To assess cluster quality, several metrics are examined, including spike waveforms, firing rate stability, autocorrelograms, cross-correlograms, and the spatial distribution of spikes across recording channels. Clusters showing highly similar waveform characteristics and correlated firing patterns may be merged, while clusters contaminated by noise or recording artifacts can be excluded [50].

Manual inspection remains the gold standard because it allows the experimenter to evaluate complex cases that automated algorithms may misclassify. However, the increasing use of high-density probes, capable of recording hundreds of neurons simultaneously, has made manual curation a major bottleneck in large-scale electrophysiological studies [53].

2. AIM OF THE WORK

The work described in this thesis was carried out at the ***Institut des Maladies Neurodégénératives*** **(IMN)**, Bordeaux Neurocampus, France. The aim of this project was to characterize the electrophysiological responses of Arkypallidal and Prototypic neurons to dopaminergic replacement therapy using in vivo Neuropixels recordings combined with optogenetic phototagging, in a mouse model of Parkinson's disease. Particular attention was given to Arkypallidal neurons, as previous work from the laboratory demonstrated that the Arkypallidal activation suppresses motor behavior [31]. Furthermore, calcium imaging experiments indicated that Arkypallidal neurons become strongly reduced following levodopa (L-DOPA) administration, raising important questions regarding the electrophysiological mechanisms underlying this response. To achieve this objective, different laser stimulation intensities were applied to determine the minimum light intensity required to reliably activate Arkypallidal neurons and to characterize their responsiveness to antidromic stimulation. This approach allowed the identification of phototagged Arkypallidal neurons and provided a baseline measure of their excitability before pharmacological treatment. Following L-DOPA administration, neuronal activity was monitored to verify whether the inhibition previously observed with calcium imaging experiments corresponded to a genuine reduction in neuronal firing. While calcium imaging suggested that Arkypallidal neurons become less active after dopaminergic treatment, the electrophysiological mechanisms underlying this response remained unknown. The principal objective of this study was therefore to investigate the mechanism responsible for the reduction in Arkypallidal activity after L-DOPA administration. In particular, the study aimed to assess whether changes in the responsiveness of Arkypallidal neurons to optogenetic stimulation, together with the activity of Prototypic neurons, could provide insight into the mechanisms contributing to this inhibition. To this end, optogenetic stimulation was repeated using progressively increasing laser intensities following L-DOPA administration while the activity of both Arkypallidal and Prototypic neurons was simultaneously evaluated. Based on previous findings indicating that Prototypic neurons provide inhibitory input to Arkypallidal neurons [32], these cells were considered a strong candidate source of the increased inhibition observed after dopamine replacement.

3. METHODS AND MATERIALS

3.1 Animal Models

Experimental procedures were carried out on 5 males (weight: 20-40 g) and 1 female (approximately 20 g) mice. All animals received a unilateral 6-hydroxydopamine (**6-OHDA**) lesion, a well-established model of Parkinson's disease that induces degeneration of the nigrostriatal dopaminergic pathway and results in characteristic motor asymmetries that can be assessed behaviorally [24].

To selectively target Arkypallidal neurons, **FoxP2-Cre** transgenic mice were used in combination with a Cre-dependent adeno-associated viral (AAV) vector encoding the opsin ChrimsonR fused to mRuby (FoxP2-Cre::AAV-DIO-Chrimson-mRuby). The Double-Floxed Inverted Orientation (DIO) configuration restricts opsin expression to Cre-expressing cells, thereby enabling selective labeling and manipulation of FoxP2-positive Arkypallidal neurons.

3.2 Photo-tagging to identify Arkypallidal neurons

To identify Arkypallidal neurons in extracellular *in vivo* electrophysiological recordings, FoxP2-Cre mice were injected with a Cre-dependent AAV encoding either **ChrimsonR** (n = 4 mice) or **ChETA** (n = 2 mice), light-sensitive opsins activated by red and blue light, respectively. Because Cre recombinase expression is driven by the FoxP2 promoter, opsin expression was restricted to Arkypallidal neurons.

As illustrated in Figure 12A, Crimson- and chETA-positive units can be identified based on their responses to brief pulses of red or blue light, respectively. In this project, as shown in figure 12B, an **antidromic** laser stimulation was used [54]. Light was delivered above the post-synaptic region of Arkypallidal neurons (by targeting the striatum), eliciting action potentials that propagated back to the soma. This approach minimized the recording artifacts commonly associated with direct optogenetic stimulation at the recording site while allowing reliable identification of Arkypallidal neurons.

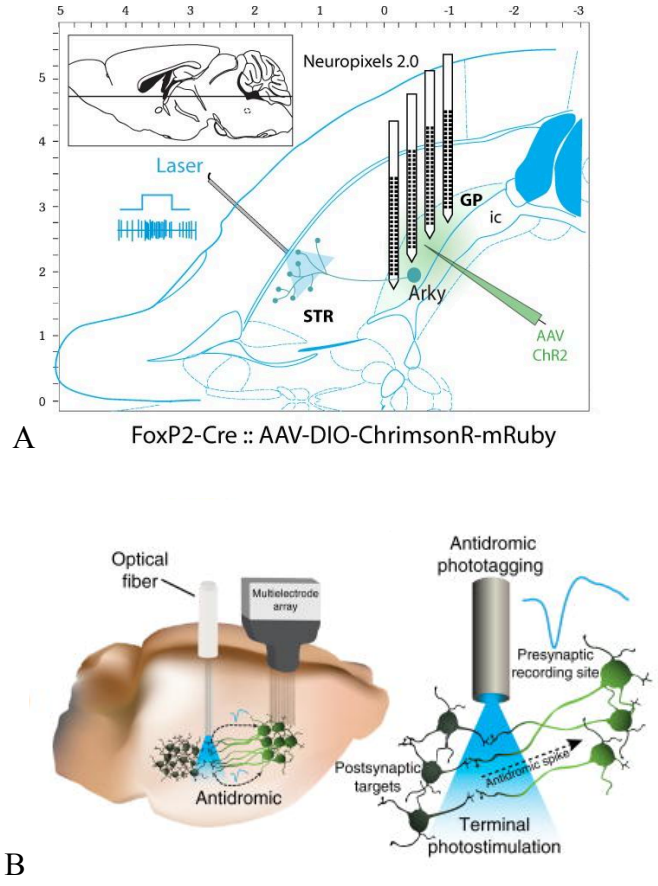

Jennings & Stuber, 2013

Figure 12. ***A)*** *Experimental approach used for Arkypallidal neuron identification. A Cre-dependent AAV encoding an opsin was injected into the GPe, resulting in selective expression in Arkypallidal neurons. Antidromic photostimulation was delivered to Arkypallidal terminals in the striatum (STR), while neuronal activity was simultaneously recorded in the GPe using a Neuropixels probe.* ***B)*** *Schematic illustration of the antidromic phototagging strategy used to identify ChrimsonR- and ChETA-expressing neurons based on their responses to brief pulses of red and blue light, respectively.*

3.3 Protocols

The same experimental protocol was applied across all animals. For each recording session, laser stimulation was delivered using a standardized gradual increase in light intensity. This approach was adopted because the threshold for optogenetic activation may vary across neurons due to several factors, including differences in Chrimson expression levels, variability in baseline neuronal activity and membrane excitability, and changes in the physiological state of the neurons following L-DOPA administration. In particular, neurons that are strongly suppressed after dopamine

replacement may require higher light intensities to elicit reliable responses. Using multiple stimulation intensities therefore ensured a more comprehensive assessment of neuronal responsiveness. However, the duration of stimulation and the number of repetitions varied between animals according to the experimental requirements. An example of the stimulation protocol is shown in Figure 13.

To assess the effects of dopaminergic replacement on neuronal activity, **levodopa** (12 mg/kg) was administered during the recording session. Electrophysiological recordings were then continued for at least 30 minutes following injection to capture the peak effects of the treatment. **Saline** injections were performed as control experiments to verify that any observed changes in neuronal activity were attributable to levodopa administration rather than to the injection procedure itself or other nonspecific factors.

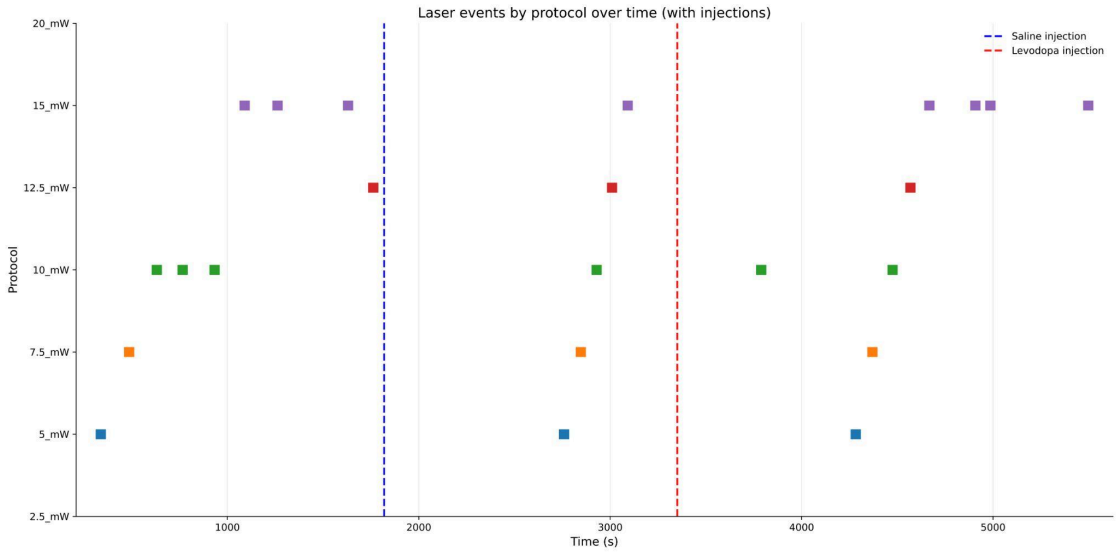

Figure 13. *Representative experimental protocol showing the timing of laser stimulation, saline injection, and levodopa administration. The x axis indicates time (s), while the y axis represents the stimulation intensity applied during the recording session. Colored blocks indicate the number of repetitions for each stimulation intensity. The blue and red vertical lines mark the time points of saline and levodopa injections, respectively.*

3.4 Recording system

Before the recording, mice were anesthetized with isoflurane and then maintained with urethane throughout the recording. After having fixed mice on a stereotaxic frame (Fig. 14A), neuronal activity was recorded using a **Neuropixels 2.0** high-density multichannel probe. Signals were acquired at a sampling rate of **30 kHz** on the **384** active recording channels. In addition, four auxiliary analog channels were recorded simultaneously, corresponding to the electrocorticography (ECoG) signal, laser stimulation trigger, synchronization signal, and injection timing, resulting in a total of 388 acquired channels. The GPe had been previously targeted during surgery. Since the GPe is tilted relative to the brain axes, the probe was inserted in the GPe with an angulation of 45°, in order to maximize the number of channels crossing it.

Following probe implantation, a stabilization period was allowed to minimize the effects of tissue displacement and electrode drift that may occur during insertion [52].

Simultaneously with GPe recordings, electrocorticogram (ECoG) activity was recorded to monitor cortical brain activity throughout the experiment.

The Neuropixels probe was connected to the **OneBox** acquisition system, a USB3 device that can acquire data from 2 headstages and transfer the data to the recording computer via a USB 3.0 connection, acting as hardware interface between the probe and the acquisition computer. Data acquisition was performed using **SpikeGLX** software (Fig. 14B), used to configure probe settings, monitor neural signals in real time, synchronize acquisition with external devices, and record electrophysiological data to disk. The software generated binary data files and associated metadata files.

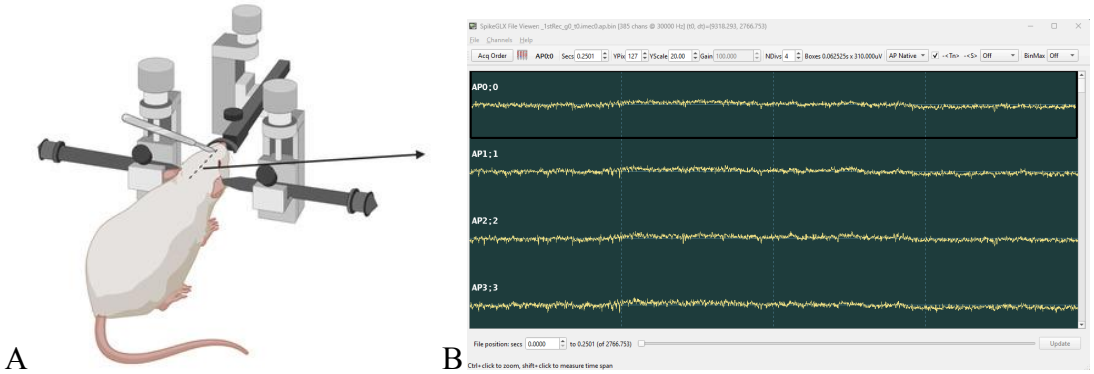

Figure 14. *Recording acquisition setup.* ***A)*** *Mouse positioned in a stereotaxic frame during electrophysiological recordings from the GPe.* ***B)*** *Representative screenshot of the SpikeGLX interface displaying raw electrophysiological signals acquired with the Neuropixels probe.*

3.5 Perfusion

At the end of the recording session, mice were deeply anesthetized and transcardially perfused with phosphate-buffered saline (PBS). Brains were subsequently collected and post-fixed in 4% PFA for histological processing. Histological analyses were performed to verify the accuracy of the targeting of the recorded brain regions.

3.6 Data analysis

Following data acquisition, the raw electrophysiological recordings were preprocessed using custom Python scripts based on the SpikeInterface framework. The **preprocessing** pipeline consisted of: 1) phase-shift correction, 2) band-pass filtering between 300 and 6000 Hz, 3) automatic detection and removal of noisy channels using a coherence and power spectral density (PSD)-based approach, and 4) local common referencing to minimize shared electrical noise. The resulting preprocessed recordings were stored in Zarr format and subsequently used for **spike sorting**, through a standardized pipeline. This automated workflow relies on **Kilosort4** (see Section 1.7.1, *Kilosort4*) to detect spikes and cluster them into putative neuronal units. The sorted data were subsequently used for manual curation and quality control.

3.6.1 Manual curation

Following automated spike sorting, all recordings underwent manual curation using **Phy** (Fig. 15), an open-source Python software designed for the visualization and curation of extracellular electrophysiological recordings obtained with high-density probes such as Neuropixels. Phy is compatible with the output generated by several spike-sorting algorithms, including Kilosort, and allows the user to inspect, merge, split, or discard clusters based on multiple electrophysiological features.

The aim of manual curation was to improve the accuracy of spike sorting by correcting errors that can occur during the automatic clustering process, such as the splitting of spikes from a single neuron into multiple clusters, merging of spikes from different neurons into the same cluster, or the inclusion of noise and recording artifacts.

The principal views used during curation are summarized below.

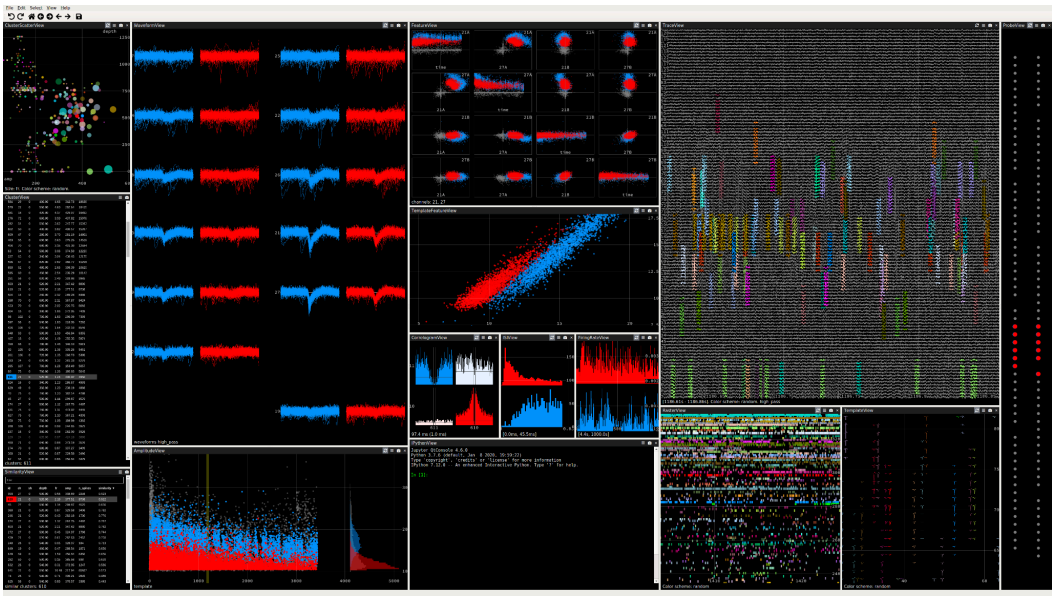

Source: Interactive visualization - phy

Figure 15. *Graphical user interface of Phy used for manual curation of spike-sorted data. The interface displays multiple visualization panels, which are used to evaluate cluster quality.*

- **The ClusterScatter view**

  This view provides a two-dimensional representation of all clusters based on selected parameters such as spike amplitude, recording depth, or firing rate. This visualization helps identify outlier clusters and assists in the rapid exploration of the dataset.

- **The cluster view**

  The Cluster view shows the list of all clusters in the dataset created by Kilosort, together with different parameters describing their properties. These include: the id of the cluster (**id**); channel with the largest spike amplitude (**ch**); the similarity score between clusters (**sh**); the probe depth of that channel (**depth**); the average firing rate (number of spikes per second) produced by that cluster during the recording (**fr**); the or median amplitude of individual spikes relative to the template (**amp**); number of spikes assigned to the cluster (**n_spikes**); **Amplitude**, that refers to the peak-to-trough amplitude of the cluster's template waveform on the main channel (the channel where the spike is largest); the contamination percentage (**ContamPct**); the automatic label assigned by Kilosort that indicates how the algorithm itself classified the cluster before manual curation (**KSLabel: good** means cluster likely corresponds to a well-isolated single neuron; **mua** is multi-unit activity, meaning that spikes from multiple neurons mixed). Moreover, it is possible to change the labels and add parameters.

  These parameters provide an initial assessment of cluster quality and facilitate the selection of candidate units for further inspection.

- **The similarity view**

  This view ranks clusters according to their waveform similarity. This information is useful for identifying clusters that may originate from the same neuron and therefore should be merged following manual inspection.

- **The amplitude view**

  This view plots spike amplitude as a function of recording time. This visualization allows the detection of electrode drift or instability during the

recording. Stable clusters typically exhibit relatively constant spike amplitudes over time, whereas abrupt amplitude changes or non-Gaussian distributions may indicate missing spikes or sorting errors.

- **The waveform view**

  This view shows the waveforms of a selection of spikes, on the relevant channels (based on amplitude and proximity to the peak waveform amplitude channel). Consistency of waveform shape throughout the recording suggests that spikes originate from a single neuron, whereas the presence of markedly different waveforms within the same cluster may indicate incorrect clustering.

- **The correlogram and ISI view**

  The **Autocorrelogram (ACG)** displays the temporal distribution of spikes generated by the same neuron. The x-axis represents the time lag (ms) between pairs of spikes, while the y-axis indicates the number of spike pairs occurring at each time lag. The **Inter-spike Interval (ISI) histogram** represents the distribution of time intervals between consecutive spikes generated by the same neuron. The x-axis corresponds to the inter-spike interval (ms), whereas the y-axis represents the number of intervals within each time bin.

  They were principally used to evaluate refractory period violations. A well-isolated single neuron should exhibit very few or no spikes within the refractory period (approximately 1–2 ms). An excess of short inter-spike intervals generally indicates contamination by spikes from multiple neurons.

  The **Cross-correlogram (CCG)** was also inspected when comparing two clusters. Similar firing patterns or characteristic dips around zero lag may suggest that the clusters belong to the same neuron and should therefore be merged.

- **The Firing rate view**

  This view shows the firing rate of the neurons across time in the recording.

- **The Feature view**

  This view displays the principal component (PC) features extracted from the spike waveforms of the selected clusters during spike sorting (see Section 1.7, *Spike Sorting*). These features are represented in a reduced-dimensional space, allowing visualization of cluster separation. Well-isolated neurons appear as compact clusters, whereas multiple separate clouds suggest poor cluster separation or contamination by spikes from different neurons.

- **The trace view**

  This displays the filtered extracellular recordings together with the detected spikes assigned to each cluster. This view was used to verify that detected spikes corresponded to genuine extracellular events and were correctly aligned with the recorded signal.

- **The Probe map view**

  The Probe map shows the spatial arrangement of recording sites on the Neuropixels probe and highlights the channels contributing to each cluster. This information facilitates the evaluation of the anatomical location and spatial extent of recorded units.

During manual curation, clusters were accepted as '**good**' single units only when they displayed stable waveform morphology, minimal refractory period violations, low contamination, clear separation from neighboring clusters in feature space and a frequency of at least 2 Hz. Clusters showing unstable waveforms, excessive refractory period violation or clear recording artifacts were discarded. When two clusters displayed highly similar waveforms, ACG and firing properties, they were merged into a single unit.

3.6.2 Classification of Arkypallidal and Prototypic neurons

Following spike sorting and manual curation, individual GPe neurons were classified as Arkypallidal or Prototypic based on their electrophysiological properties together with their optogenetic responses. Phy was used to inspect waveform characteristics, spike timing, firing activity, ACG and ISI trend, amplitude response to photostimulation and levodopa injection. These criteria enabled the identification of optogenetically tagged Arkypallidal neurons and their distinction from non-tagged Arkypallidal neurons and Prototypic neurons.

3.6.3 Final validation of optotagged Arkypallidal neurons

Following spike sorting and manual curation, the clusters classified as putative single units were further analyzed to identify optotagged Arkypallidal neurons. Neural spike times (AP timestamps) and the timing of laser stimulation (OBX/TTL timestamps) were recorded independently and therefore required temporal alignment before analysis.

After synchronization of AP and OBX timestamps, each unit was evaluated according to three criteria: response reliability, rate ratio, and response latency. **Reliability** was defined as the percentage of laser pulses that evoked at least one action potential. The **rate ratio** was calculated as the ratio between the firing rate during the laser stimulation period and the baseline firing rate immediately preceding stimulation. Units with a rate ratio ≥ 5 were considered to show a robust optogenetic response. **Response latency** was defined as the time between laser onset and the first evoked spike; only neurons with a latency between 5 and 10 ms were considered candidate Arkypallidal neurons.

The list of candidate optotagged units obtained from this analysis was subsequently re-examined in Phy. Waveform shape, spike amplitude stability, frequency were inspected to exclude optogenetic artifacts or poorly isolated clusters. Only neurons that fulfilled both the quantitative optotagging criteria and the manual quality-control criteria were included in the final dataset.

4. RESULTS

4.1 Identification of Arkypallidal and Prototypic neurons

Following automated spike sorting with Kilosort4, approximately 400 clusters were identified per recording, including both putative single units and multi-unit activity (MUA). After manual curation in Phy, only about 20% of these clusters were retained for further analysis, corresponding to well-isolated single units that fulfilled the quality criteria described in the Methods section. This stringent selection minimized the inclusion of false-positive units and poorly isolated clusters.

Among the curated neurons, only a small proportion were identified as optogenetically tagged Arkypallidal neurons (‘Arky’), whereas the remaining units were classified either as Prototypic neurons (‘Proto’) or just ‘good’ units. This finding was expected because, as explained in the Introduction, Arkypallidal neurons constitute only about 20% of the GPe neuronal population [55] and, in addition, not all Arkypallidal neurons were successfully transduced or phototagged. Overall, approximately one to two Arkypallidal neurons were identified per animal.

Figure 16 shows an example of Prototypic (Fig. 16A) and Arkypallidal (Fig. 16B) neurons following manual curation in Phy. As expected, Prototypic neurons displayed a relatively high and regular spontaneous firing rate (approximately 20–80 Hz), reflected by the periodic peaks in the autocorrelogram and the narrow distribution of inter-spike intervals. In contrast, Arkypallidal neurons exhibited a slower and more irregular firing pattern, typically ranging between 3 and 10 Hz.

As described in the Methods section, well-isolated units are generally expected to exhibit a clear refractory period in the autocorrelogram, indicating that spikes originate from a single neuron. However, this criterion requires particular consideration for optogenetically tagged neurons. Because laser pulses evoke precisely timed action potentials, phototagged Arkypallidal neurons frequently exhibit a prominent peak close to time zero in both the autocorrelogram (ACG) and inter-spike interval (ISI) distribution, indicated by the arrows. This early peak reflects the optogenetically evoked responses, whereas the longer tail corresponds to the spontaneous, irregular firing activity occurring outside laser stimulation.

Therefore, identification of Arkypallidal neurons did not rely solely on ACG and ISI profiles. Additional parameters, including firing rate, spike amplitude stability, waveform shape, and firing pattern throughout the recording, were systematically inspected to distinguish genuine phototagged neurons from optogenetic stimulation artifacts, which typically exhibited extremely low spontaneous firing rates (generally below 1–2 Hz) and inconsistent spike characteristics.

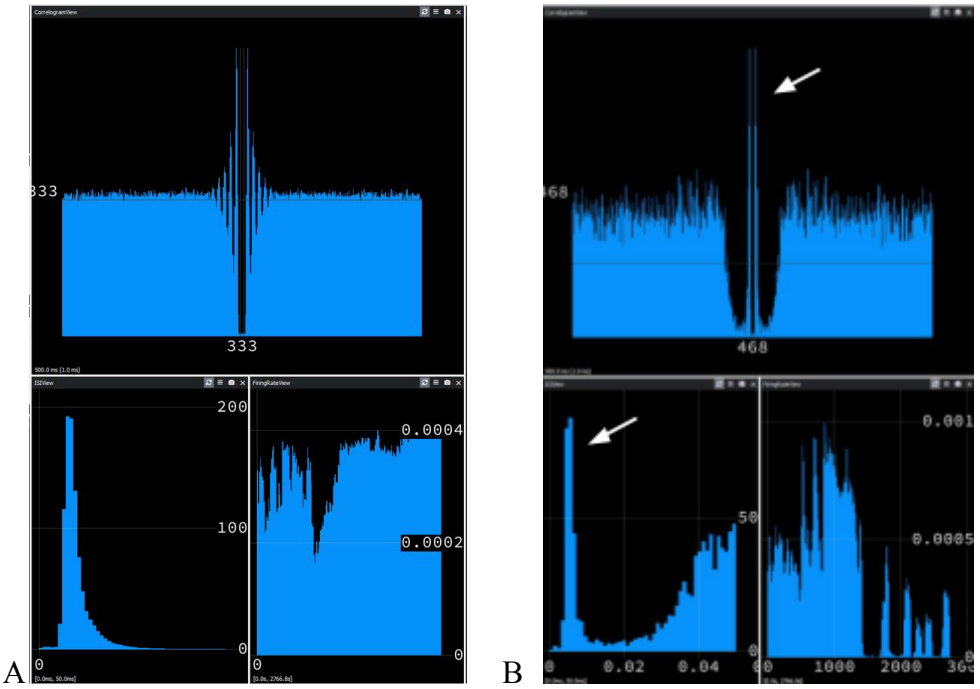

Figure 16. *Representative Phy views of Prototypic and Arkypallidal neurons after manual curation.* ***A)*** *Autocorrelogram (ACG, top), inter-spike interval (ISI, bottom left), and firing rate (bottom right) of a Prototypic (Proto) neuron.* ***B)*** *Corresponding views for an optogenetically identified Arkypallidal (Arky) neuron. The white arrows indicate the peaks around time zero (ACG) and at short interspike intervals (ISI), corresponding to spikes evoked by optogenetic stimulation.*

The final identification of Arkypallidal neurons was obtained by combining electrophysiological features observed during manual curation with phototagging parameters extracted from TTL-aligned laser stimulation data.

4.2 Optotagging response of Arkypallidal neurons

Following their identification, phototagged Arkypallidal neurons were aligned to the onset of the laser pulse in order to characterize their responses to antidromic optogenetic stimulation.

Figure 17 shows a representative raster plot of a phototagged Arkypallidal neuron before L-DOPA administration. As the laser intensity increased, the probability of evoking action potentials also increased, indicating a progressive recruitment of neuronal responses with stronger optical stimulation. The lower panel shows the corresponding peri-stimulus time histogram (PSTH), illustrating the increase in firing probability with increasing laser intensity.

A detectable response was observed at a laser intensity of **2.5 mW**, although only a small fraction of laser pulses elicited spikes. In contrast, stimulation intensities of **7.5 mW and above** produced a marked increase in firing reliability, suggesting that this range is sufficient to consistently activate Arkypallidal neurons under the present experimental conditions.

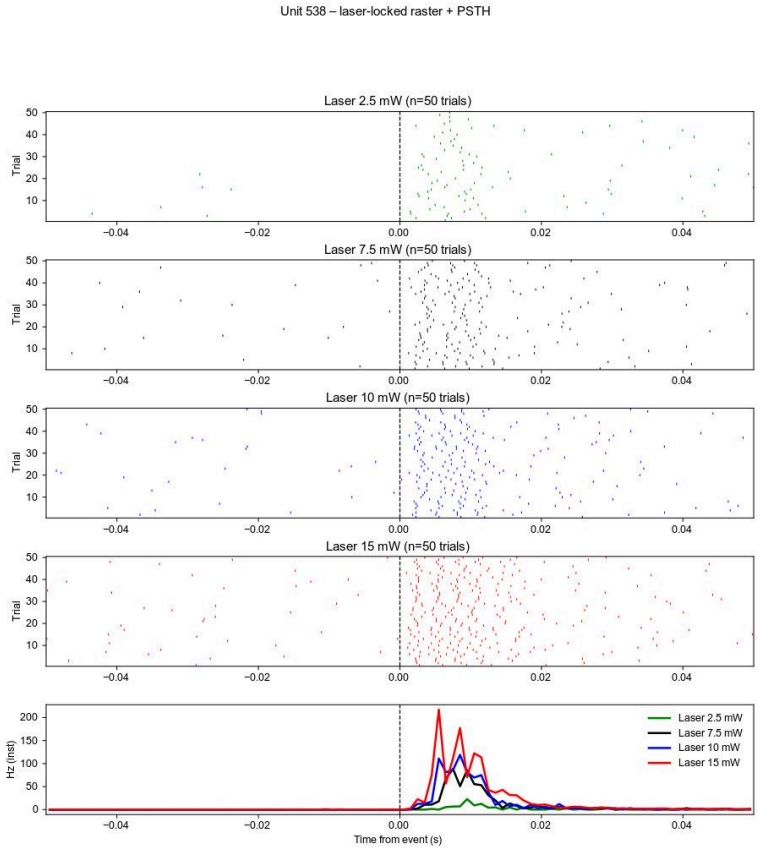

Figure 17. *Raster plot and Peristimulus time histogram (PSTH) showing the response of a phototagged Arky neuron to the increasing laser stimulation before L-DOPA administration. The 4 top graphs are raster plots: the y axis represents the trials, meaning all the time the laser is on; the x axis is the time relative to the laser (before, during and after the stimulation), where time 0 corresponds to the laser onset. The bottom graph is a PSTH: the y axis is firing rate (Hz), the x axis is time relative to the stimulus.*

To confirm that laser-evoked spikes originated from the recorded neuron rather than from stimulation artifacts, spike waveforms recorded during laser stimulation were compared with spontaneous spikes occurring outside the stimulation period. As shown in Figure 18, the average waveform morphology remained unchanged before, during, and after optogenetic stimulation (±100 ms relative to laser onset), indicating that the optogenetically evoked spikes corresponded to the same neuronal unit throughout the recording.

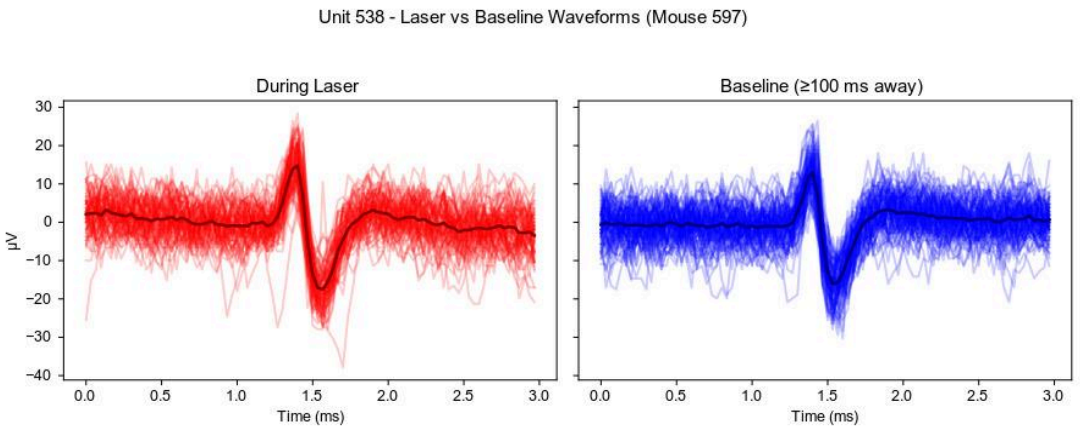

Figure 18. *Representation of average waveform shape of an Arky neuron during and outside the laser stimulation. The left panel represents the waveform shape during laser stimulation; the right panel shows the waveform shape 100 ms before and after the stimulation.*

4.3 Arkypallidal activity following L-DOPA administration

Following the identification and validation of Arkypallidal neurons, their electrophysiological response to L-DOPA administration was evaluated. As shown in Figure 19, Arkypallidal neurons exhibited a marked reduction in spontaneous firing following L-DOPA injection. In addition, their responses to optogenetic stimulation were substantially reduced compared with the pre-treatment condition, showing only slight increases during laser pulses.

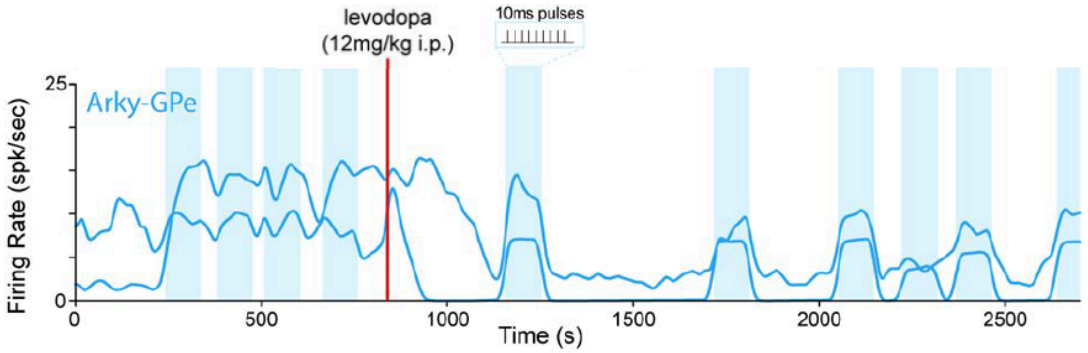

Figure 19. *Representative firing rate traces of two Arkypallidal (Arky) neurons recorded in a Parkinsonian mouse before and after L-DOPA administration. The x axis represents the time (s), while the y axis represents the firing rate (spikes/s). The red vertical line indicates the time of levodopa injection; the blue bars indicate the timing of optogenetic laser stimulation. From left to right, the laser stimulation intensities under basal conditions are 10 mW, 5 mW, 2.5 mW, 12.5 mW. Following L-DOPA administration, the stimulation intensities are 10 mW, 10 mW, 10 mW, 2.5 mW, 5 mW, 10 mW.*

To further characterize this effect, raster plots and peri-stimulus time histograms (PSTHs) were generated for individual Arkypallidal neurons at different laser stimulation intensities before and after L-DOPA administration.

In several neurons recorded from different mice, laser-evoked responses were markedly attenuated following L-DOPA treatment, consistent with previous calcium imaging observations (Fig. 20).

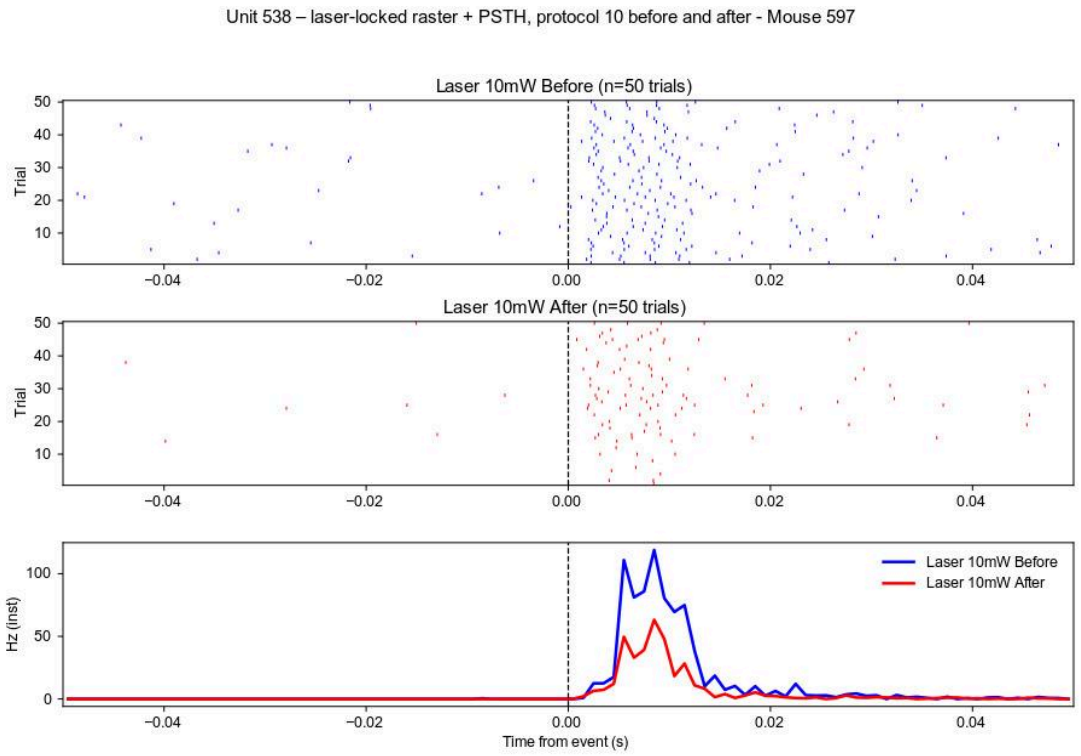

Figure 20. *Raster plot and Peristimulus time histogram (PSTH) showing the response of an Arky neuron to the 10 mW optogenetic stimulation before (blue line) and after (red line) L-DOPA injection. Each row of the raster plot represents one trial, and time 0 corresponds to laser onset. The PSTH shows the average firing rate across trials. Compared with the basal condition, the response to laser stimulation is markedly reduced following L-DOPA administration.*

To exclude the possibility that these changes resulted from recording instability or the experimental protocol itself, saline injections were used as a control. As shown in Figure 21, neuronal activity remained comparable between basal and saline conditions, whereas a clear reduction in firing was observed only after L-DOPA administration, supporting the conclusion that the observed inhibition was specifically associated with dopaminergic treatment.

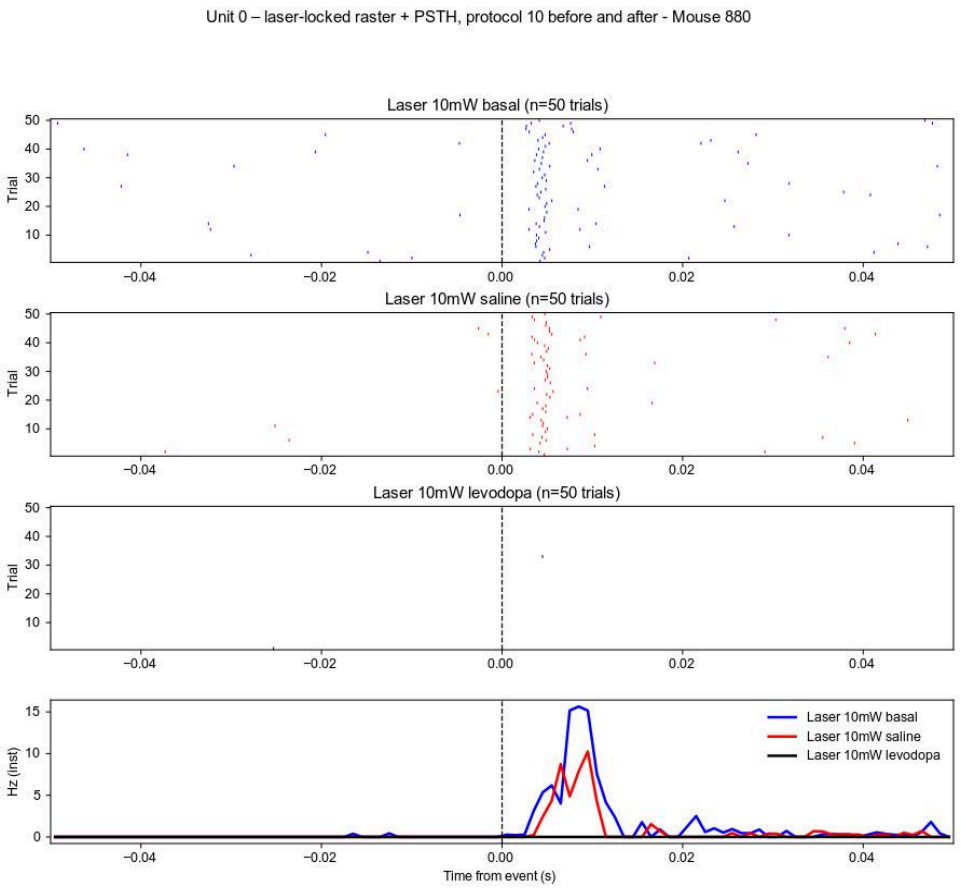

Figure 21. *Raster plot and Peristimulus time histogram (PSTH) of an Arky neuron, showing its response to the 10 mW optogenetic stimulation under basal condition (blue line), after saline injection (red line) and after L-DOPA injection (black line). The response to laser stimulation is preserved after saline injection but is markedly reduced following L-DOPA administration.*

Moreover, the effects of different stimulation intensities were also investigated. At 2.5 mW, Arkypallidal neurons showed little or no response following L-DOPA administration (Fig. 22A). Increasing the stimulation intensity to 10 mW (Fig. 22B) and 12.5 mW (Fig. 22C) produced only limited recovery of the laser-evoked response, suggesting that stronger optical stimulation was insufficient to fully restore neuronal activity.

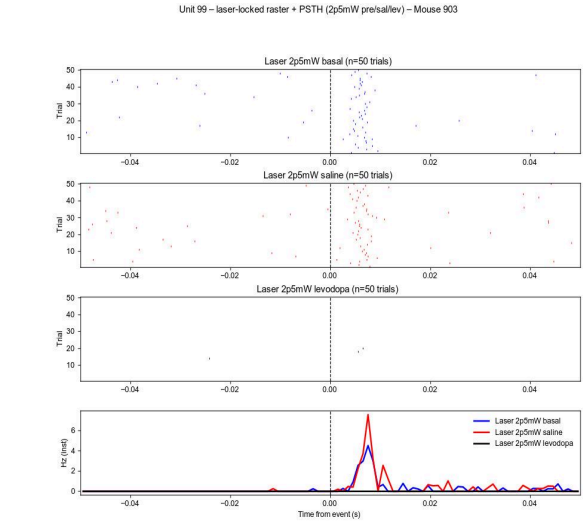

A

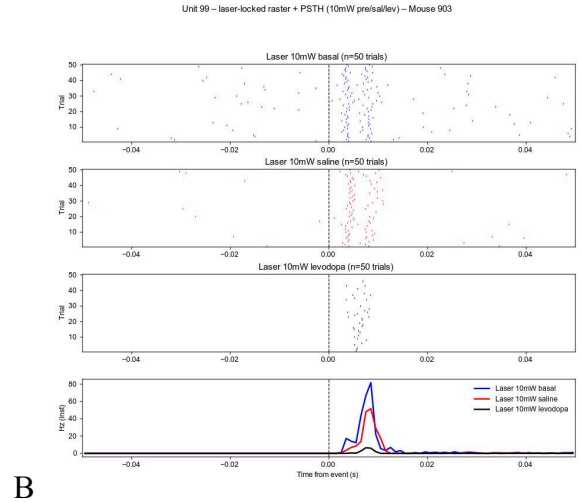

B

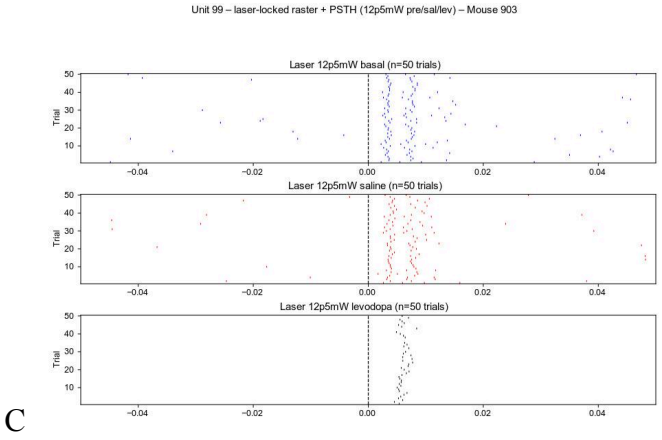

C

Figure 22. *Raster plot and Peristimulus time histogram (PSTH) showing the response of an Arky neuron to optogenetic stimulation at 2.5 mW (A), 10 mW (B) and 12.5 mW (C) under basal condition (blue line), after saline injection (red line) and after L-DOPA injection (black line). While the neuron responds robustly to increasing laser intensities under basal conditions and after saline injection, its response is markedly reduced following L-DOPA administration, with only a weak residual response at higher stimulation intensities.*

Although the majority of Arkypallidal neurons displayed this characteristic reduction in activity, a small number of recordings showed atypical responses. For example, in one recording, neuronal activity decreased following both saline and L-DOPA injections (Fig. 23A), suggesting possible recording instability, such as electrode drift. In another case (Fig. 23B), the apparent increase in laser-evoked activity after L-DOPA was not consistent with the expected physiological response and, following inspection in Phy, was considered likely to reflect an optogenetic recording artifact rather than genuine neuronal activity. These examples highlight the importance of combining automated analyses with careful manual validation of waveform stability, spike amplitude, contamination, and cluster quality.

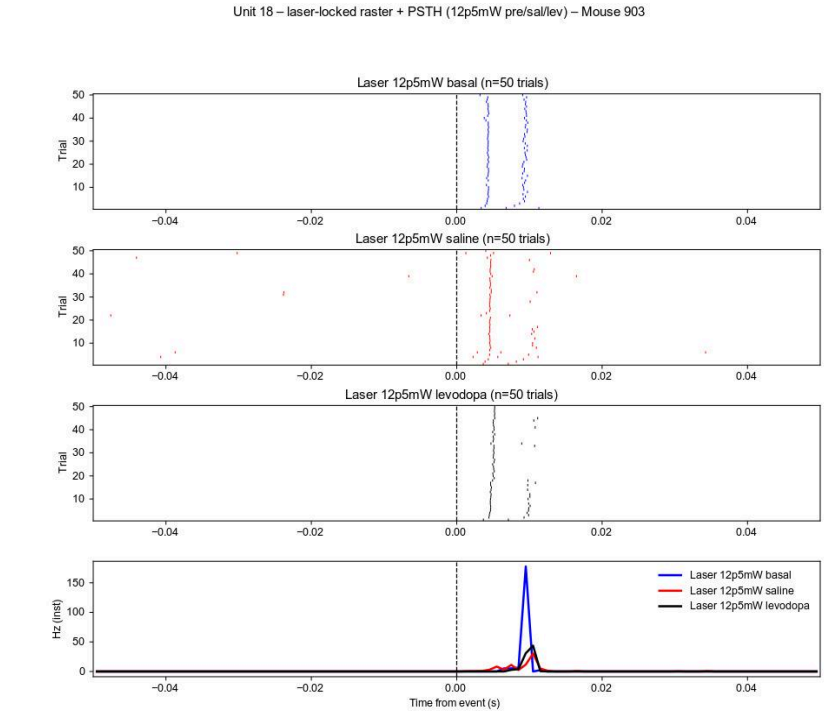

A

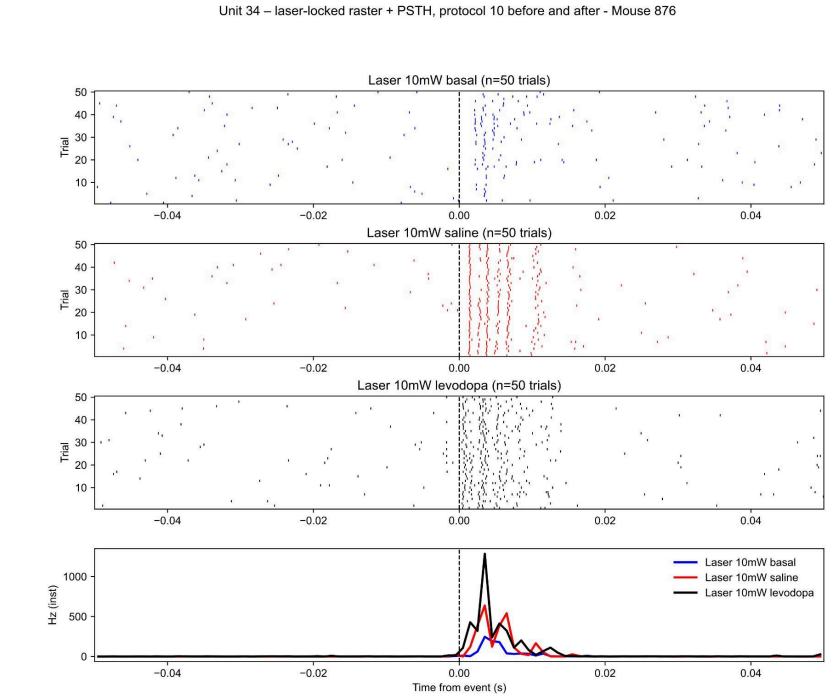

B

Figure 23. *Raster plot and Peristimulus time histogram (PSTH) of two Arky neurons recorded from two different mice, showing atypical responses to optogenetic stimulation under basal conditions (blue line), after saline injection (red line) and after L-DOPA injection (black line).* ***A)*** *Decrease in firing activity following both saline and L-DOPA administration, likely reflecting recording instability or electrode drift. B) Abnormally increased firing activity after L-DOPA administration, most likely attributable to optogenetic stimulation artifacts.*

To further assess the reduction in Arkypallidal activity after L-DOPA administration, violin plots were generated using all well-isolated Arkypallidal neurons. Figure 24A shows that the overall firing rate significantly decreased following L-DOPA injection. Similarly, the firing rate during laser stimulation was reduced after L-DOPA (Fig. 24B), as was the firing rate measured outside the stimulation period (Fig. 24C). The mean inter-spike interval (ISI) significantly increased after L-DOPA (Fig. 24D), indicating that spikes occurred farther apart in time and reflecting a lower firing rate.

Because the mean can be influenced by extreme values, the median ISI was also calculated. Although the median ISI showed a tendency to increase after L-DOPA (Fig. 24E), this change did not reach statistical significance. Likewise, the coefficient of variation (CV) of the ISI, used to assess firing regularity, exhibited a slight increase after L-DOPA (Fig. 24F), but this difference was also not statistically significant. Together, these findings indicate that L-DOPA primarily reduced the overall firing activity of Arkypallidal neurons without significantly altering the temporal pattern or regularity of their spike discharge.

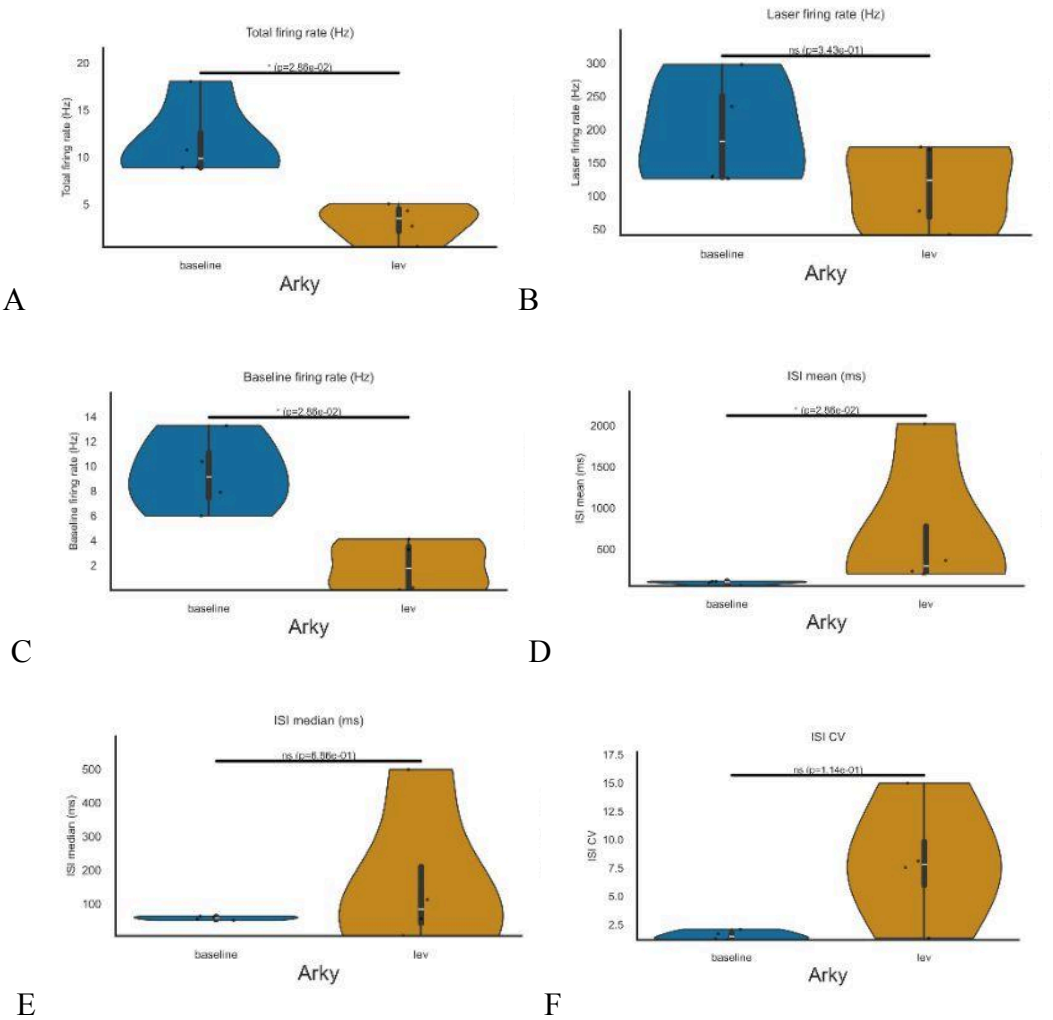

Figure 24. *Violin plots summarizing the electrophysiological properties of well-isolated Arkypallidal neurons (from different mice) before and after L-DOPA administration.* ***A)*** *Total firing rate during and outside the laser stimulation (*p=0.0286).* ***B)*** *Firing rate during laser stimulation (p=0.343).* ***C)*** *Firing rate outside laser stimulation (*p=0.0286).* ***D)*** *Mean inter-spike interval (ISI) (*p=0.0286).* ***E)*** *Median ISI (p=0.686).* ***F)*** *Coefficient of variation (CV) of the ISI (p=0.114).*

Overall, these findings demonstrate that L-DOPA markedly suppresses the activity of Arkypallidal neurons, confirming previous observations obtained with calcium imaging. Furthermore, the persistence of reduced responses even at higher stimulation intensities suggests that the decrease in activity cannot be fully explained by a reduction in intrinsic excitability alone and is consistent with the presence of increased inhibitory input from other neuronal populations.

4.4 Prototypic activity following L-DOPA administration

To further investigate the mechanisms underlying the reduction in Arkypallidal activity after L-DOPA administration, the electrophysiological activity of Prototypic neurons was also examined.

The same analyses performed for Arkypallidal neurons were applied to representative Prototypic neurons (Fig. 25). In contrast to Arkypallidal neurons, Prototypic neurons exhibited an increase in firing rate following L-DOPA administration and showed no detectable response to optogenetic stimulation. These observations are consistent with the selective phototagging of Arkypallidal neurons and suggest that Prototypic neurons were not directly activated by the laser stimulation.

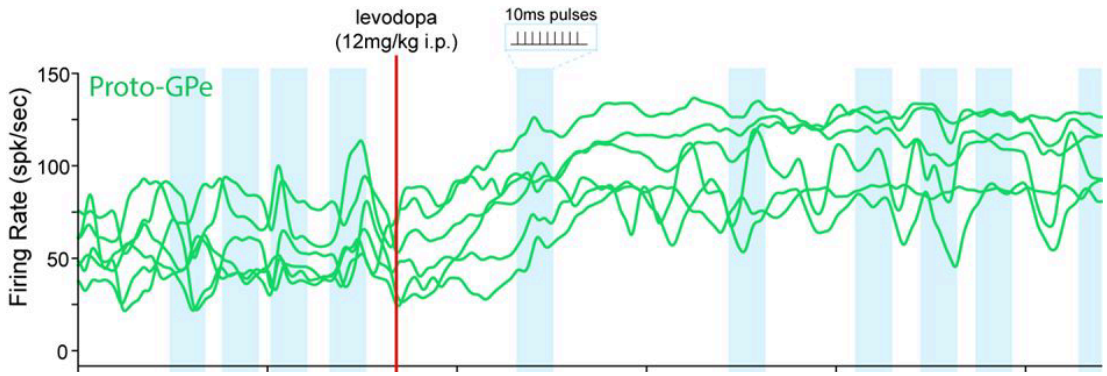

Figure 25. *Representative firing rate traces of Prototypic (Proto) neurons recorded in a Parkinsonian mouse before and after L-DOPA administration. The x axis represents the time (s), while the y axis represents the firing rate (spikes/s). The red vertical line indicates the time of levodopa injection; the blue bars indicate the timing of optogenetic laser stimulation.*

To assess whether these changes were consistent across animals, the electrophysiological properties of well-isolated Prototypic neurons from different mice were compared before and after L-DOPA administration using violin plots (Fig. 26). The overall firing rate significantly increased after L-DOPA injection (Fig. 26A). Similarly, firing rates measured during (Fig. 26B) and outside (Fig. 26C) laser stimulation were higher following L-DOPA administration than under basal conditions.

The mean (Fig. 26D) and median (Fig. 26E) inter-spike intervals (ISI) both decreased after L-DOPA administration, indicating that Prototypic neurons fired more frequently. Although most Prototypic neurons maintained relatively low ISI coefficient of variation (CV) values (Fig. 26F), a subset displayed a marked increase in firing variability, resulting in a broader distribution of ISI CV after treatment. These findings indicate that, despite the overall increase in firing rate, spike timing became more variable in part of the Prototypic neuron population.

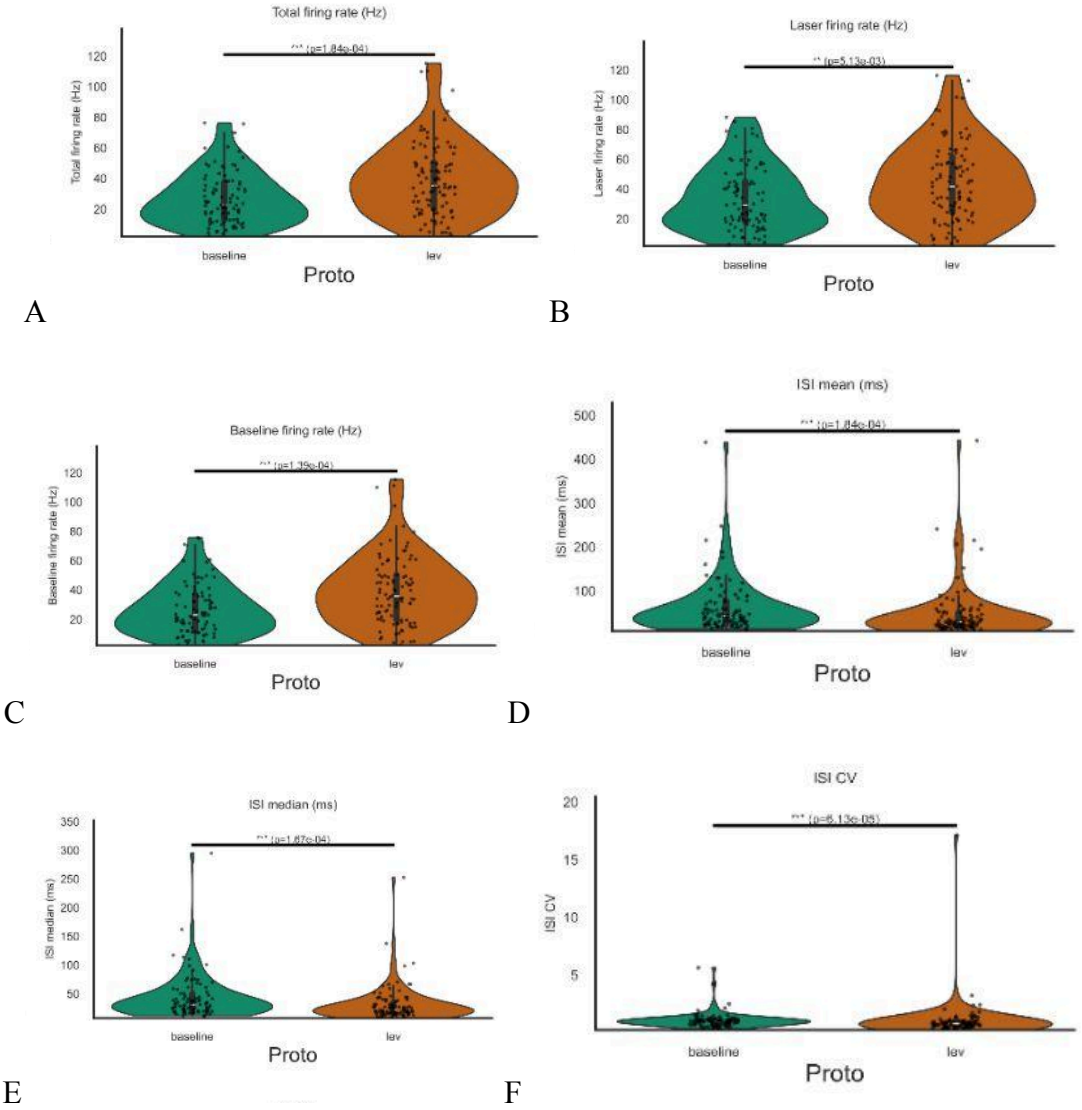

Figure 26. *Violin plots summarizing the electrophysiological properties of Prototypic neurons (from different mice) before and after L-DOPA administration.* ***A)*** *Total firing rate during and outside the laser stimulation (***p=0.000184).* ***B)*** *Firing rate during laser stimulation (**p=0.00513).* ***C)*** *Firing rate outside laser stimulation (***p=0.000139).* ***D)*** *Mean inter-spike-interval (ISI) (***p=0.000184).* ***E)*** *Median ISI (***p=0.000167).* ***F)*** *Coefficient of variation (CV) of the ISI (***p=0.0000613).*

Overall, these findings indicate that L-DOPA exerts opposite effects on the two major neuronal populations of the GPe, decreasing the activity of Arkypallidal neurons while increasing the firing of Prototypic neurons.

4.5 Comparison of Arkypallidal and Prototypic neuronal activity

Following the confirmation that Arkypallidal and Prototypic neurons exhibit opposite responses to L-DOPA administration, a comparative analysis of the electrophysiological properties of the two neuronal populations was performed under basal conditions and after dopaminergic treatment. Previous studies have suggested that Prototypic neurons may exert inhibitory control over Arkypallidal neurons; therefore, comparing the activity of these two populations may provide further insight into this potential relationship.

To provide an overall representation of their responses, the average firing activity of well-isolated Arkypallidal and Prototypic neurons recorded from the same mice was analyzed. As observed for individual neurons, the population average revealed a marked increase in Prototypic firing and a concomitant decrease in Arkypallidal activity following L-DOPA administration (Fig. 27).

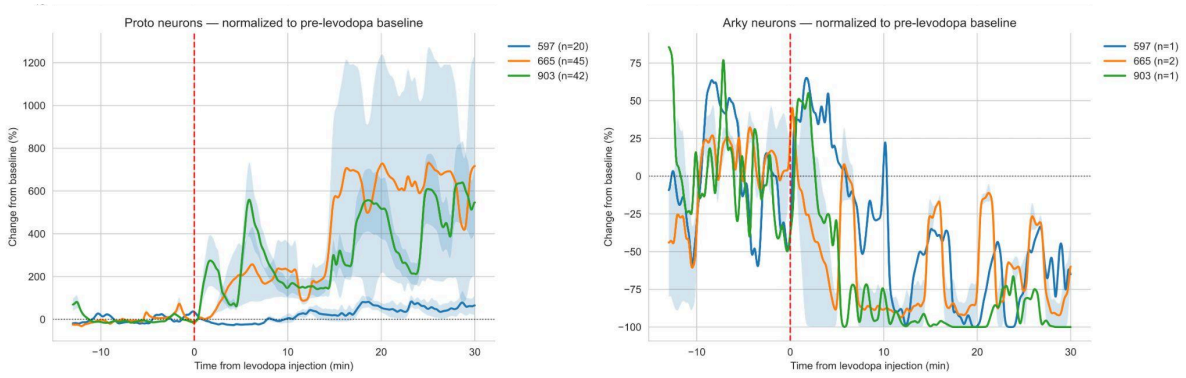

Figure 27. *Representative changes in firing rate of Proto (left) and Arky (right) neurons before and after L-DOPA administration. Vertical dashed line indicates the time of injection of L-DOPA (time = 0 s). The y axis represents the firing change relative to the baseline period. Each colored trace corresponds to the neurons of a specific mouse.*

Violin plots were then generated to compare the electrophysiological properties of both neuronal populations before (Fig. 28) and after (Fig. 29) L-DOPA administration.

Under basal conditions, Prototypic neurons exhibited significantly higher total firing rates (Fig. 28A) and baseline firing rates outside laser stimulation (Fig. 28C), consistent with their characteristic tonic firing pattern. In contrast, Arkypallidal neurons displayed significantly higher firing rates during laser stimulation (Fig. 28B), reflecting their selective activation by antidromic optogenetic stimulation. Furthermore, Prototypic neurons showed significantly lower mean (Fig. 28D), median (Fig. 28E), and coefficient of variation (CV) of the inter-spike interval (ISI) (Fig. 28F), indicating that they fired at higher frequencies and with greater temporal regularity than Arkypallidal neurons.

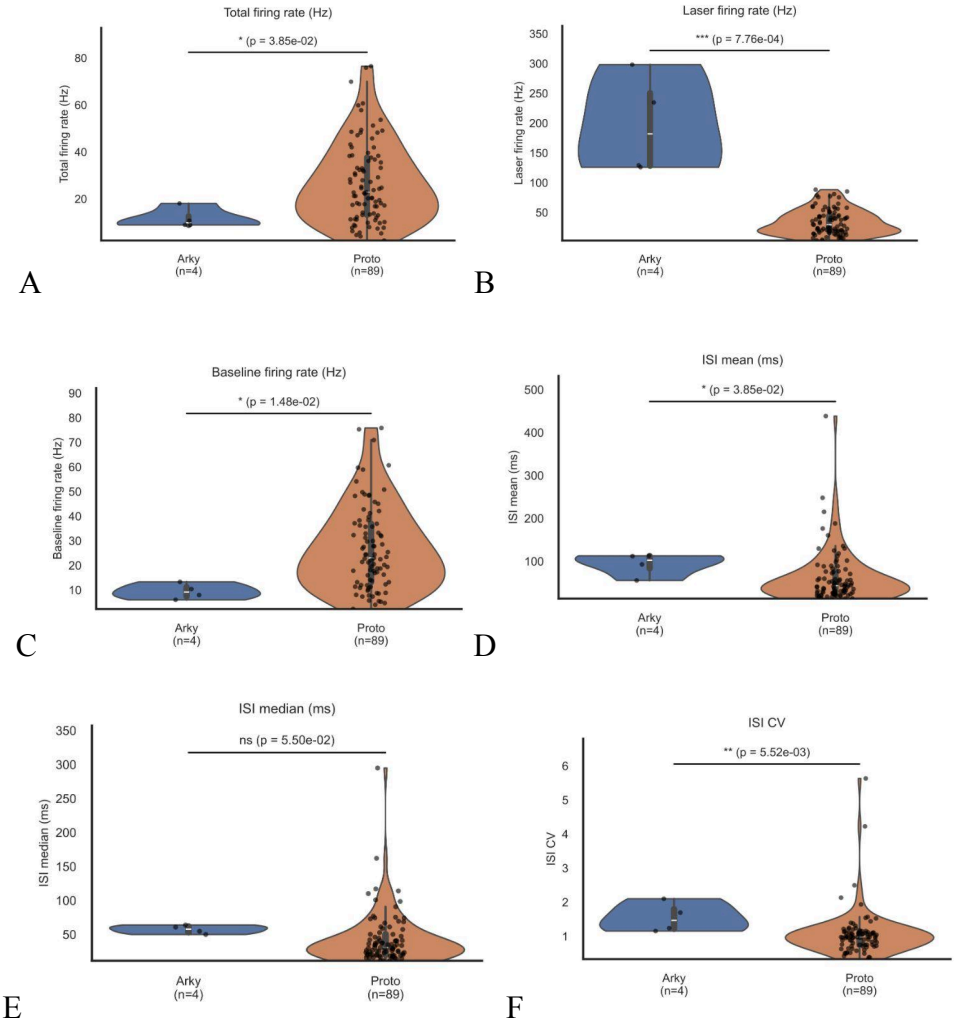

Figure 28. *Violin plots comparing the electrophysiological properties of well-isolated Arky (n = 4) and Proto (n = 89) neurons under basal conditions.* ***A)*** *Total firing rate (*p=0.0385).* ***B)*** *Firing rate during laser stimulation (***p=0.000776)* ***C)*** *Baseline firing rate outside laser stimulation (*p=0.0148).* ***D)*** *Mean inter-spike interval (ISI) (*p=0.0385).* ***E)*** *Median ISI (p=0.055).* ***F)*** *Coefficient of variation (CV) of the ISI (**p=0.00552).*

Following L-DOPA administration, the electrophysiological differences between the two neuronal populations became more pronounced. Arkypallidal neurons exhibited a marked reduction in both total firing rate (Fig. 29A) and baseline firing rate (Fig. 29C), whereas Prototypic neurons maintained significantly higher firing rates. During laser stimulation (Fig. 29B), Arkypallidal neurons still responded to optogenetic activation, although their firing rate remained substantially lower than under basal conditions, indicating a reduced responsiveness after L-DOPA treatment.

The mean (Fig. 29D) and median (Fig. 29E) ISI remained significantly lower in Prototypic neurons, consistent with their higher firing frequency. In addition, the difference in ISI coefficient of variation between the two neuronal populations became even more pronounced after L-DOPA administration (Fig. 29F; $p = 1.69 \times 10^{-4}$).

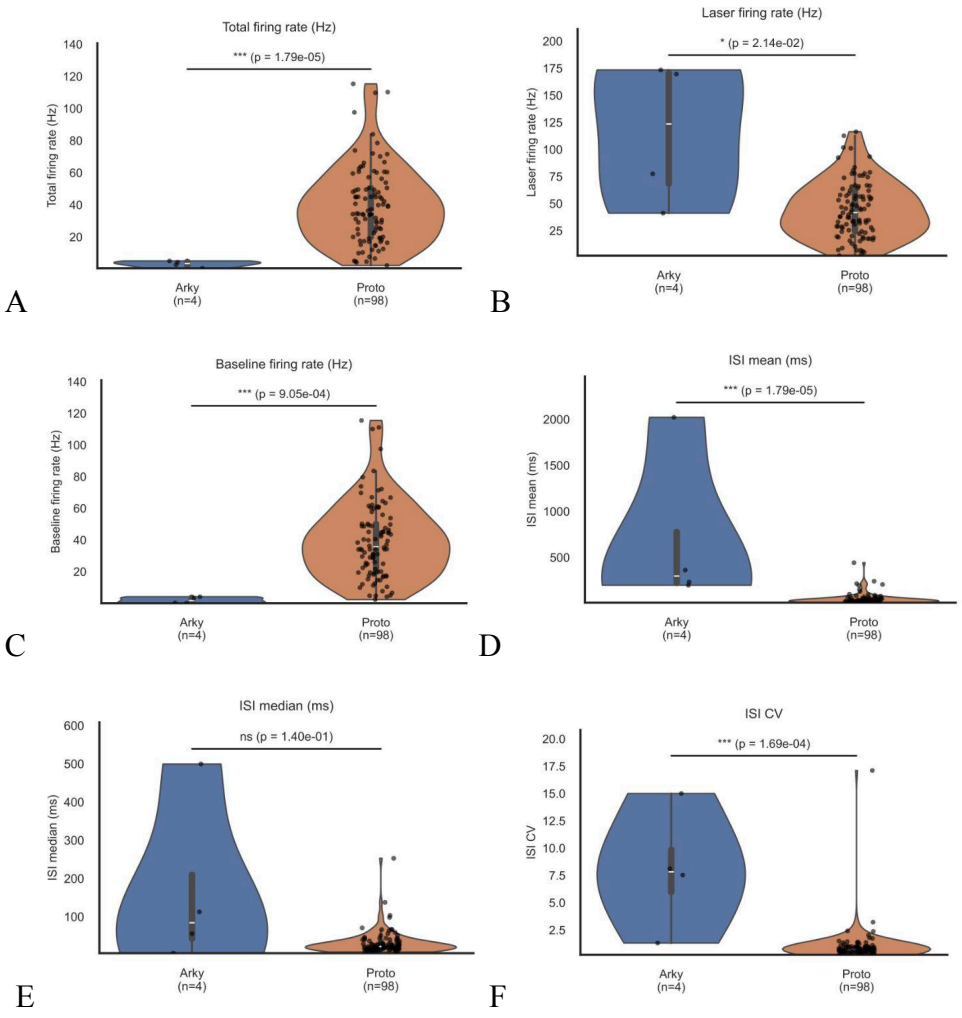

Figure 29. *Violin plots comparing the electrophysiological properties of well-isolated Arky (n = 4) and Proto (n = 98) neurons following L-DOPA administration.* ***A)*** *Total firing rate (***0.0000179).* ***B)*** *Firing rate during laser stimulation (*p=0.0214).* ***C)*** *Baseline firing rate outside laser stimulation (***p=0.000905).* ***D)*** *Mean inter-spike interval (ISI) (***p=0.0000179).* ***E)*** *Median ISI (p=0.14).* ***F)*** *Coefficient of variation (CV) of the ISI (***p=0.000169).*

Overall, these findings demonstrate that L-DOPA accentuates the distinct electrophysiological profiles of the two principal neuronal populations of the GPe. Whereas Prototypic neurons increase their firing activity after dopaminergic replacement, Arkypallidal neurons exhibit a marked reduction in activity and greater firing irregularity. These observations are consistent with the hypothesis that enhanced Prototypic neuron activity may contribute to the suppression of Arkypallidal neurons, although direct evidence of this mechanism will require further investigation.

5. DISCUSSION

Disruption of basal ganglia circuitry is a hallmark of movement disorders such as Parkinson's disease, in which the degeneration of dopaminergic neurons leads to profound alterations in neuronal activity throughout the network [56], [6], [19].

The external globus pallidus (GPe) has emerged as a key integrative nucleus composed of two major neuronal populations: Prototypic neurons, which account for approximately 80% of GPe neurons, and Arkypallidal neurons, which represent the remaining 20% [29], [34], [57], [33], [32]. Previous work from the laboratory demonstrated that activation of Arkypallidal neurons suppresses motor behavior [31], highlighting their important role in motor control. Furthermore, calcium imaging experiments suggested that Arkypallidal neurons become inhibited following L-DOPA administration in a mouse model of Parkinson's disease. However, because calcium imaging provides only an indirect measure of neuronal activity, in vivo electrophysiological recordings were required to determine whether this decrease reflected a genuine reduction in neuronal firing and to investigate the mechanisms underlying this response.

5.1 Electrophysiological confirmation of calcium imaging

Following automated spike sorting and manual curation, reliable identification and classification of Arkypallidal and Prototypic neurons were achieved (Fig. 16) based on their electrophysiological properties, including firing rate, firing pattern, autocorrelograms, inter-spike interval distributions, waveform characteristics, and optogenetic responsiveness. The combination of automated clustering with manual curation was essential to ensure the selection of well-isolated single units while minimizing contamination from multi-unit activity or spike sorting errors, as previously described for high-density electrophysiological recordings [50], [36], [49]. The use of antidromic optogenetic phototagging further increased the reliability of Arkypallidal neuron identification, allowing these neurons to be distinguished from the larger Prototypic population.

The results demonstrated that Arkypallidal neurons could be reliably activated by antidromic optogenetic stimulation without directly affecting the activity of neighboring Prototypic neurons, confirming the specificity of the phototagging strategy.

The present findings provide the first electrophysiological confirmation of previous calcium imaging observations obtained in the same laboratory, which suggested that Arkypallidal neurons become inhibited following L-DOPA administration (Fig. 19). By combining Neuropixels recordings with antidromic phototagging, the present study demonstrated that the reduction in calcium activity corresponds to a genuine decrease in the firing rate of identified Arkypallidal neurons after dopaminergic replacement therapy, in agreement with previous findings from the laboratory, whereas Prototypic neurons exhibited the opposite response, showing a significant increase in firing rate (Fig. 25).

This opposite modulation of the two principal neuronal populations of the GPe is consistent with previous electrophysiological studies describing their distinct functional roles within basal ganglia circuits [57] and supports the idea that dopamine depletion and dopamine replacement profoundly reshapes GPe network activity. [29], [58], [59], [60], [61].

5.2 Possible mechanisms underlying Arkypallidal inhibition following L-DOPA

Importantly, increasing the intensity of optogenetic stimulation after L-DOPA administration resulted in only a limited recovery of Arkypallidal responses (Fig. 21-22). Together with the marked increase in Prototypic neuron activity observed after dopamine replacement, these findings support the hypothesis that network-level inhibitory mechanisms contribute to the suppression of Arkypallidal neurons. This interpretation is consistent with previous electrophysiological studies demonstrating that local GABAergic connections within the GPe exert a strong influence on the firing activity of neighboring neurons [62]. Since Prototypic neurons are known to provide inhibitory input to Arkypallidal neurons [32], their increased activity represents a plausible mechanism underlying the reduction in Arkypallidal firing following L-DOPA administration.

Nevertheless, Prototypic neurons may not represent the only source of inhibition acting on Arkypallidal neurons after dopamine replacement. Another possible mechanism is a direct dopaminergic effect on Arkypallidal neurons through dopamine D2 receptors. Previous studies have reported the expression of D2 receptors in pallidal neurons, raising the possibility that L-DOPA may directly modulate Arkypallidal excitability [35]. In addition, recent evidence indicates that axon collaterals of direct-pathway striatal projection neurons (D1-SPNs) preferentially target Arkypallidal neurons within the external globus pallidus [34]. Because D1-SPNs become strongly activated following dopamine replacement, increased striatopallidal inhibition may also contribute to the suppression of Arkypallidal activity observed in the present study.

Although the present study does not directly demonstrate this causal relationship, the simultaneous increase in Prototypic firing and decrease in Arkypallidal activity following L-DOPA administration is compatible with this hypothesis and provides a strong basis for future investigations aimed at identifying the precise mechanisms responsible for Arkypallidal inhibition.

5.3 Functional implications for basal ganglia circuit

An important advance of the current study is the simultaneous electrophysiological characterization of both identified Arkypallidal and Prototypic neurons following L-DOPA administration.

The opposite modulation of Arkypallidal and Prototypic neurons observed following L-DOPA administration suggests that dopaminergic replacement therapy induces a substantial reorganization of neuronal activity within the external globus pallidus (GPe), with important consequences for basal ganglia circuit function. Integrating these findings with the current model of basal ganglia connectivity provides new insights into the mechanisms underlying motor recovery following dopamine replacement and the potential emergence of dyskinetic activity.

Under physiological conditions, a balance between Prototypic and Arkypallidal neuronal activity contributes to the regulation of basal ganglia output. Prototypic

neurons constitute the principal GPe output to downstream basal ganglia nuclei, whereas Arkypallidal neurons project almost exclusively back to the striatum [63], where they inhibit both striatal projection neurons and interneurons, contributing to the suppression of inappropriate motor programs [29], [55], [57], [64].

In Parkinson's disease, dopamine depletion profoundly alters the activity of basal ganglia circuits [20], [65]. The increased activity of the indirect pathway and the reduced activation of the direct pathway promote excessive inhibitory output from the basal ganglia, resulting in impaired movement initiation and bradykinesia. The present results indicate that, following L-DOPA administration, Arkypallidal neurons markedly decrease their firing while Prototypic neurons become more active. This opposite modulation is likely to alter the balance of inhibition within the GPe and its downstream targets.

A possible functional model is proposed in Figure 30, which integrates previous knowledge of basal ganglia circuitry with the new electrophysiological evidence obtained in the present study. The schematic illustrates the transition from physiological conditions to the Parkinsonian state and, finally, to the L-DOPA-treated condition. Following dopamine replacement, Prototypic neurons exhibit an increased firing rate. The enhanced activity of Prototypic neurons may strengthen local inhibitory projections within the GPe, thereby suppressing Arkypallidal neurons. Reduced Arkypallidal activity would in turn decrease pallidostriatal inhibition, contributing to the restoration of movement following L-DOPA administration.

Since L-DOPA administration increased Prototypic firing while reducing Arkypallidal activity, it is tempting to speculate that the opposite mechanism may occur following dopamine depletion, consistent with the findings of Aristieta [32]. In this scenario, reduced Prototypic activity could lead to a disinhibition of Arkypallidal neurons, thereby increasing their firing. Such a mechanism would be consistent with the proposed role of Arkypallidal neurons in movement suppression and could contribute to the hypokinetic symptoms characteristic of Parkinson's disease. However, because recordings from healthy control animals were not performed in the present study, this interpretation remains speculative and requires direct experimental validation.

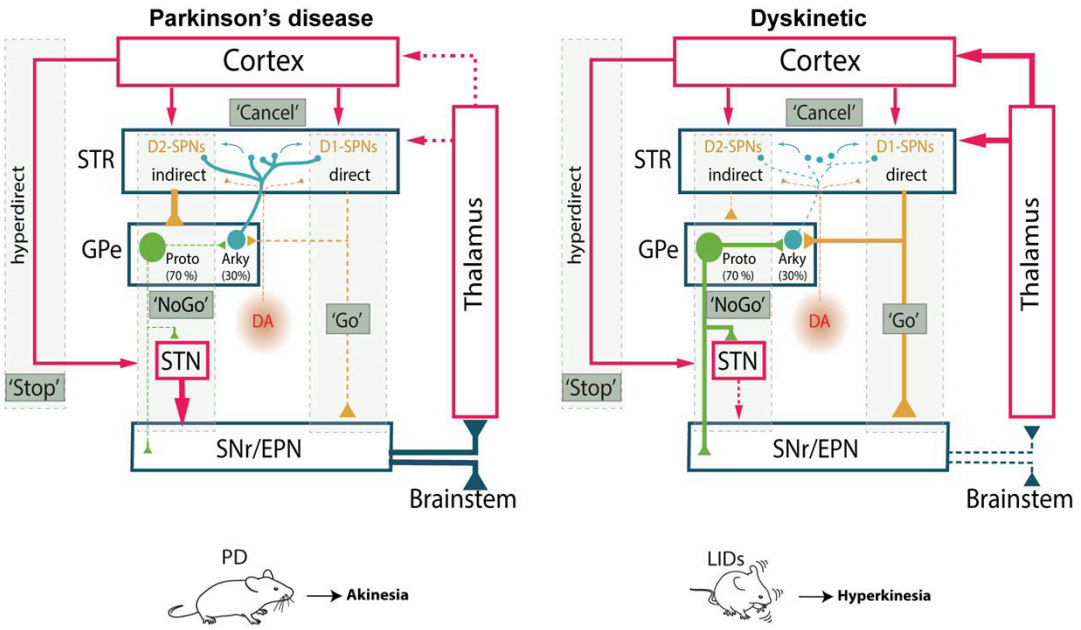

Source: Arkypallidal neurons in basal ganglia circuits: Unveiling novel pallidostriatal loops? - Guilhemsang et al., 2023

Figure 30. *Schematic representation of basal ganglia circuit change in two different conditions: Parkinson's disease (PD), levodopa-induced dyskinesia (LID). In PD (left panel), there is a hypothesized reduction of Proto-mediated inhibition leading to Arky disinhibition and increased movement suppression (akinesia). In LID (right panel), Proto activity increases, leading to a hypothesized suppression of Arky, relieving pallidostriatal inhibition and producing abnormal movement (hyperkinesia).*

5.4 Strengths, limitations and future perspectives

One of the principal strengths of the present study is the use of *in vivo* extracellular electrophysiological recordings, which provide a direct measure of neuronal firing with high temporal resolution. Compared with calcium imaging, electrophysiology allows precise quantification of action potential timing and firing patterns, thereby offering a more accurate characterization of neuronal activity [66].

In particular, these *in vivo* extracellular recordings were conducted with a modern, cutting-edge tool, that is the Neuropixels 2.0 high-density multichannel probe, which enabled the simultaneous recording of hundreds of neurons with high spatial and temporal resolution. This technology has improved the ability to investigate neuronal circuits by increasing recording yield, stability and spatial coverage compared with previous extracellular recording techniques [37], [53]. Combined with antidromic

optogenetic phototagging (Fig. 12), Neuropixels recordings allowed the reliable identification of Arkypallidal neurons while minimizing activation of neighbouring neuronal populations [54].

Moreover, the data analysis pipeline also represents a strength of this work. Automated spike sorting using Kilosort4, followed by manual curation in Phy, combined the efficiency of computational algorithms with evaluation of waveform quality, firing stability, refractory period violations and cluster isolation. This hybrid approach improves the reliability of single-unit identification [67], [68].

Despite these strengths, several limitations should be considered. Although manual curation improves spike sorting quality, it inevitably introduces a degree of subjectivity, as cluster classification depends on the interpretation of multiple electrophysiological features by the operator. Previous studies have shown that even experienced users may differ in their classification of well-isolated units and that manual curation is susceptible to errors caused by overlapping clusters, waveform variability and limitations in visualizing high-dimensional feature spaces [36], [50]. The integration of objective quality metrics and manual curation strategies may further improve reproducibility in future studies [69].

Another limitation is the relatively small sample size. Only a limited number of animals were included and, because Arkypallidal neurons represent approximately 20% of the GPe population, only one or two optogenetically identified Arkypallidal neurons were typically obtained from each recording. Although strict inclusion criteria increased confidence in the analyzed units, the reduced sample size limits the statistical power and the generalizability of the findings.

Additional limitations arise from the experimental design. Recordings were performed under anaesthesia and exclusively in hemiparkinsonian mice, without recordings from healthy control animals. Future experiments performed in awake, behaving mice, together with recordings from healthy controls, will be important to determine how the observed electrophysiological changes relate to motor behavior and to distinguish healthy from disease-related alterations and those specifically induced by dopamine replacement.

Careful interpretation is also required because extracellular recordings combined with optogenetic stimulation may be affected by stimulation artifacts or spike sorting errors, as already described. Although antidromic stimulation reduces the probability of light-induced artifacts and extensive manual curation was performed to exclude suspicious units, the possibility of residual contamination cannot be completely excluded.

Finally, the simultaneous increase in Prototypic firing and decrease in Arkypallidal activity, together with the well-established inhibitory projections from Prototypic to Arkypallidal neurons [32], strongly support the hypothesis that Prototypic neurons contribute to the inhibition of Arkypallidal neurons following L-DOPA administration. However, the present experiments do not demonstrate that Prototypic neurons are the sole source of the observed inhibition, nor do they directly prove that their increased activity is necessary to produce the reduction in Arkypallidal firing.

An important future direction would therefore be to exploit the simultaneous Neuropixels recordings obtained in this study to investigate functional connectivity between identified Prototypic and Arkypallidal neurons using cross-correlogram analyses. Detection of putative monosynaptic inhibitory interactions would provide further evidence for functional connectivity, while comparing these interactions across Parkinsonian and L-DOPA-treated conditions could reveal whether dopamine depletion or dopamine replacement modifies the probability or efficacy of Proto-to-Arky inhibition. Complementary causal experiments, such as selectively inhibiting Prototypic neurons during L-DOPA treatment using optogenetic or chemogenetic approaches, could then determine whether their activity is required for the suppression of Arkypallidal neurons.

Conversely, selective optogenetic activation of Arkypallidal neurons in dyskinetic animals would determine whether restoring Arkypallidal activity attenuates L-DOPA-induced dyskinesia, thereby supporting a causal role for Arkypallidal suppression in dyskinetic motor symptoms.

6. CONCLUSION

This study provides the first electrophysiological confirmation that Arkypallidal neurons reduce their firing following L-DOPA administration in a mouse model of Parkinson's disease.

The results further demonstrate a significant increase in the activity of Prototypic neurons after L-DOPA treatment. The simultaneous decrease in Arkypallidal activity and increase in Prototypic firing, together with the known inhibitory connectivity between these neuronal populations, suggest that Prototypic neurons may contribute to the suppression of Arkypallidal neurons following dopamine replacement.

Overall, these findings provide new insight into the functional organization of the external globus pallidus and its role in the response to dopaminergic therapy. They contribute to a better understanding of the basal ganglia circuit and provide a basis for future studies investigating the cellular and synaptic mechanisms underlying motor control, Parkinson's disease, and L-DOPA-induced adaptations.

7. BIBLIOGRAPHY

[1] R. H. Roth e J. B. Ding, «Cortico-basal ganglia plasticity in motor learning», *Neuron*, vol. 112, fasc. 15, pp. 2486–2502, ago. 2024, doi: 10.1016/j.neuron.2024.06.014.

[2] J. Cox e I. B. Witten, «Striatal circuits for reward learning and decision-making», *Nat. Rev. Neurosci.*, vol. 20, fasc. 8, pp. 482–494, ago. 2019, doi: 10.1038/s41583-019-0189-2.

[3] L. R. Squire, «Memory systems of the brain: A brief history and current perspective», *Neurobiol. Learn. Mem.*, vol. 82, fasc. 3, pp. 171–177, nov. 2004, doi: 10.1016/j.nlm.2004.06.005.

[4] J. W. Mink, «THE BASAL GANGLIA: FOCUSED SELECTION AND INHIBITION OF COMPETING MOTOR PROGRAMS», *Prog. Neurobiol.*, vol. 50, fasc. 4, pp. 381–425, nov. 1996, doi: 10.1016/S0301-0082(96)00042-1.

[5] E. R. Kandel, J. Koester, S. Mack, e S. Siegelbaum, A c. di, *Principles of neural science*, Sixth edition. New York: McGraw Hill, 2021.

[6] A. B. Nelson e A. C. Kreitzer, «Reassessing Models of Basal Ganglia Function and Dysfunction», *Annu. Rev. Neurosci.*, vol. 37, fasc. 1, pp. 117–135, lug. 2014, doi: 10.1146/annurev-neuro-071013-013916.

[7] R. L. Albin, A. B. Young, e J. B. Penney, «The functional anatomy of basal ganglia disorders», *Trends Neurosci.*, vol. 12, fasc. 10, pp. 366–375, gen. 1989, doi: 10.1016/0166-2236(89)90074-X.

[8] S. Elias, Y. Ritov, e H. Bergman, «Balance of Increases and Decreases in Firing Rate of the Spontaneous Activity of Basal Ganglia High-Frequency Discharge Neurons», *J. Neurophysiol.*, vol. 100, fasc. 6, pp. 3086–3104, dic. 2008, doi: 10.1152/jn.90714.2008.

[9] J. L. Lanciego, N. Luquin, e J. A. Obeso, «Functional Neuroanatomy of the Basal Ganglia», *Cold Spring Harb. Perspect. Med.*, vol. 2, fasc. 12, pp. a009621–a009621, dic. 2012, doi: 10.1101/cshperspect.a009621.

[10] C. D. Courtney, A. Pamukcu, e C. S. Chan, «Cell and circuit complexity of the external globus pallidus», *Nat. Neurosci.*, vol. 26, fasc. 7, pp. 1147–1159, lug. 2023, doi: 10.1038/s41593-023-01368-7.

[11] «emedicine.medscape.com_article_1831191-print».

[12] R. B. Postuma *et al.*, «MDS clinical diagnostic criteria for Parkinson's disease», *Mov. Disord.*, vol. 30, fasc. 12, pp. 1591–1601, ott. 2015, doi: 10.1002/mds.26424.

[13] J. Jankovic, «Parkinson's disease: clinical features and diagnosis», *J. Neurol. Neurosurg. Psychiatry*, vol. 79, fasc. 4, pp. 368–376, apr. 2008, doi: 10.1136/jnnp.2007.131045.

[14] R. Chen *et al.*, «Clinical neurophysiology of Parkinson's disease and parkinsonism», *Clin. Neurophysiol. Pract.*, vol. 7, pp. 201–227, 2022, doi: 10.1016/j.cnp.2022.06.002.

[15] C. Blauwendraat, M. A. Nalls, e A. B. Singleton, «The genetic architecture of Parkinson's disease», *Lancet Neurol.*, vol. 19, fasc. 2, pp. 170–178, feb. 2020, doi: 10.1016/S1474-4422(19)30287-X.

[16] L. M. Bekris, I. F. Mata, e C. P. Zabetian, «The Genetics of Parkinson Disease», *J. Geriatr. Psychiatry Neurol.*, vol. 23, fasc. 4, pp. 228–242, dic. 2010, doi: 10.1177/0891988710383572.

[17] U. C. Dash *et al.*, «Oxidative stress and inflammation in the pathogenesis of neurological disorders: Mechanisms and implications», *Acta Pharm. Sin. B*, vol. 15, fasc. 1, pp. 15–34, gen. 2025, doi: 10.1016/j.apsb.2024.10.004.
[18] J. H. Kordower, Y. Chu, R. A. Hauser, T. B. Freeman, e C. W. Olanow, «Lewy body–like pathology in long-term embryonic nigral transplants in Parkinson's disease», *Nat. Med.*, vol. 14, fasc. 5, pp. 504–506, mag. 2008, doi: 10.1038/nm1747.
[19] M. DeLong e T. Wichmann, «Update on models of basal ganglia function and dysfunction», *Parkinsonism Relat. Disord.*, vol. 15, pp. S237–S240, dic. 2009, doi: 10.1016/S1353-8020(09)70822-3.
[20] L. V. Kalia e A. E. Lang, «Parkinson's disease», *The Lancet*, vol. 386, fasc. 9996, pp. 896–912, ago. 2015, doi: 10.1016/S0140-6736(14)61393-3.
[21] L. M. Suarez, O. Solis, C. Aguado, R. Lujan, e R. Moratalla, «L-DOPA Oppositely Regulates Synaptic Strength and Spine Morphology in D1 and D2 Striatal Projection Neurons in Dyskinesia», *Cereb. Cortex*, vol. 26, fasc. 11, pp. 4253–4264, ott. 2016, doi: 10.1093/cercor/bhw263.
[22] T. Fieblinger *et al.*, «Cell type-specific plasticity of striatal projection neurons in parkinsonism and L-DOPA-induced dyskinesia», *Nat. Commun.*, vol. 5, fasc. 1, p. 5316, ott. 2014, doi: 10.1038/ncomms6316.
[23] S. Pandey e P. Srivanitchapoom, «Levodopa-induced dyskinesia: Clinical features, pathophysiology, and medical management», *Ann. Indian Acad. Neurol.*, vol. 20, fasc. 3, p. 190, 2017, doi: 10.4103/aian.AIAN_239_17.
[24] A. Galvan, A. Devergnas, e T. Wichmann, «Alterations in neuronal activity in basal ganglia-thalamocortical circuits in the parkinsonian state», *Front. Neuroanat.*, vol. 9, feb. 2015, doi: 10.3389/fnana.2015.00005.
[25] Q. Cui *et al.*, «Striatal Direct Pathway Targets Npas1^{+} Pallidal Neurons», *J. Neurosci.*, vol. 41, fasc. 18, pp. 3966–3987, mag. 2021, doi: 10.1523/JNEUROSCI.2306-20.2021.
[26] C. Kellendonk *et al.*, «DOPAMINE D2 RECEPTORS REGULATE THE ANATOMICAL BALANCE OF BASAL GANGLIA CIRCUITRY», *Schizophr. Res.*, vol. 153, p. S70, apr. 2014, doi: 10.1016/S0920-9964(14)70227-0.
[27] N. N. Foster *et al.*, «The mouse cortico–basal ganglia–thalamic network», *Nature*, vol. 598, fasc. 7879, pp. 188–194, ott. 2021, doi: 10.1038/s41586-021-03993-3.
[28] S. Okamoto *et al.*, «Overlapping Projections of Neighboring Direct and Indirect Pathway Neostriatal Neurons to Globus Pallidus External Segment», *iScience*, vol. 23, fasc. 9, p. 101409, set. 2020, doi: 10.1016/j.isci.2020.101409.
[29] N. Mallet *et al.*, «Dichotomous Organization of the External Globus Pallidus», *Neuron*, vol. 74, fasc. 6, pp. 1075–1086, giu. 2012, doi: 10.1016/j.neuron.2012.04.027.
[30] V. Lilascharoen *et al.*, «Divergent pallidal pathways underlying distinct Parkinsonian behavioral deficits», *Nat. Neurosci.*, vol. 24, fasc. 4, pp. 504–515, apr. 2021, doi: 10.1038/s41593-021-00810-y.
[31] N. Mallet *et al.*, «Arkypallidal Cells Send a Stop Signal to Striatum», *Neuron*, vol. 89, fasc. 2, pp. 308–316, gen. 2016, doi: 10.1016/j.neuron.2015.12.017.
[32] A. Aristieta *et al.*, «A Disynaptic Circuit in the Globus Pallidus Controls Locomotion Inhibition», *Curr. Biol.*, vol. 31, fasc. 4, pp. 707-721.e7, feb. 2021, doi: 10.1016/j.cub.2020.11.019.

[33] L. Guilhemsang e N. P. Mallet, «Arkypallidal neurons in basal ganglia circuits: Unveiling novel pallidostriatal loops?», *Curr. Opin. Neurobiol.*, vol. 84, p. 102814, feb. 2024, doi: 10.1016/j.conb.2023.102814.
[34] M. Ketzef e G. Silberberg, «Differential Synaptic Input to External Globus Pallidus Neuronal Subpopulations In Vivo», *Neuron*, vol. 109, fasc. 3, pp. 516-529.e4, feb. 2021, doi: 10.1016/j.neuron.2020.11.006.
[35] B. R. Hoover e J. F. Marshall, «Molecular, chemical, and anatomical characterization of globus pallidus dopamine D2 receptor mRNA‐containing neurons», *Synapse*, vol. 52, fasc. 2, pp. 100–113, mag. 2004, doi: 10.1002/syn.20007.
[36] K. D. Harris, D. A. Henze, J. Csicsvari, H. Hirase, e G. Buzsáki, «Accuracy of Tetrode Spike Separation as Determined by Simultaneous Intracellular and Extracellular Measurements», *J. Neurophysiol.*, vol. 84, fasc. 1, pp. 401–414, lug. 2000, doi: 10.1152/jn.2000.84.1.401.
[37] G. Buzsáki, «Large-scale recording of neuronal ensembles», *Nat. Neurosci.*, vol. 7, fasc. 5, pp. 446–451, mag. 2004, doi: 10.1038/nn1233.
[38] M. S. Lewicki, «A review of methods for spike sorting: the detection and classification of neural action potentials».
[39] E. N. Brown, R. E. Kass, e P. P. Mitra, «Multiple neural spike train data analysis: state-of-the-art and future challenges», *Nat. Neurosci.*, vol. 7, fasc. 5, pp. 456–461, mag. 2004, doi: 10.1038/nn1228.
[40] N. A. Steinmetz *et al.*, «Neuropixels 2.0: A miniaturized high-density probe for stable, long-term brain recordings», *Science*, vol. 372, fasc. 6539, p. eabf4588, apr. 2021, doi: 10.1126/science.abf4588.
[41] M. Pachitariu, N. A. Steinmetz, S. N. Kadir, M. Carandini, e K. D. Harris, «Fast and accurate spike sorting of high-channel count probes with KiloSort».
[42] R. Q. Quiroga, «Spike sorting», *Curr. Biol.*, vol. 22, fasc. 2, pp. R45–R46, gen. 2012, doi: 10.1016/j.cub.2011.11.005.
[43] «obd_ch3_2».
[44] C. Pouzat, O. Mazor, e G. Laurent, «Using noise signature to optimize spike-sorting and to assess neuronal classification quality», *J. Neurosci. Methods*, vol. 122, fasc. 1, pp. 43–57, dic. 2002, doi: 10.1016/S0165-0270(02)00276-5.
[45] R. Q. Quiroga, Z. Nadasdy, e Y. Ben-Shaul, «Unsupervised Spike Detection and Sorting with Wavelets and Superparamagnetic Clustering», *Neural Comput.*, vol. 16, fasc. 8, pp. 1661–1687, ago. 2004, doi: 10.1162/089976604774201631.
[46] D. L. Donoho, «De-noising by soft-thresholding», *IEEE Trans. Inf. Theory*, vol. 41, fasc. 3, pp. 613–627, mag. 1995, doi: 10.1109/18.382009.
[47] J. C. Letelier e P. P. Weber, «Spike sorting based on discrete wavelet transform coefficients», *J. Neurosci. Methods*, vol. 101, fasc. 2, pp. 93–106, set. 2000, doi: 10.1016/S0165-0270(00)00250-8.
[48] M. Pachitariu, S. Sridhar, J. Pennington, e C. Stringer, «Spike sorting with Kilosort4», *Nat. Methods*, vol. 21, fasc. 5, pp. 914–921, mag. 2024, doi: 10.1038/s41592-024-02232-7.
[49] J. J. Jun *et al.*, «Fully integrated silicon probes for high-density recording of neural activity», *Nature*, vol. 551, fasc. 7679, pp. 232–236, nov. 2017, doi: 10.1038/nature24636.
[50] C. Rossant *et al.*, «Spike sorting for large, dense electrode arrays», *Nat. Neurosci.*, vol. 19, fasc. 4, pp. 634–641, apr. 2016, doi: 10.1038/nn.4268.

[51] D. N. Hill, S. B. Mehta, e D. Kleinfeld, «Quality Metrics to Accompany Spike Sorting of Extracellular Signals», *J. Neurosci.*, vol. 31, fasc. 24, pp. 8699–8705, giu. 2011, doi: 10.1523/JNEUROSCI.0971-11.2011.
[52] H. G. Rey, C. Pedreira, e R. Quian Quiroga, «Past, present and future of spike sorting techniques», *Brain Res. Bull.*, vol. 119, pp. 106–117, ott. 2015, doi: 10.1016/j.brainresbull.2015.04.007.
[53] I. H. Stevenson e K. P. Kording, «How advances in neural recording affect data analysis», *Nat. Neurosci.*, vol. 14, fasc. 2, pp. 139–142, feb. 2011, doi: 10.1038/nn.2731.
[54] J. H. Jennings e G. D. Stuber, «Tools for Resolving Functional Activity and Connectivity within Intact Neural Circuits», *Curr. Biol.*, vol. 24, fasc. 1, pp. R41–R50, gen. 2014, doi: 10.1016/j.cub.2013.11.042.
[55] P. D. Dodson *et al.*, «Distinct Developmental Origins Manifest in the Specialized Encoding of Movement by Adult Neurons of the External Globus Pallidus», *Neuron*, vol. 86, fasc. 2, pp. 501–513, apr. 2015, doi: 10.1016/j.neuron.2015.03.007.
[56] P. Redgrave *et al.*, «Goal-directed and habitual control in the basal ganglia: implications for Parkinson's disease», *Nat. Rev. Neurosci.*, vol. 11, fasc. 11, pp. 760–772, nov. 2010, doi: 10.1038/nrn2915.
[57] A. Abdi *et al.*, «Prototypic and Arkypallidal Neurons in the Dopamine-Intact External Globus Pallidus», *J. Neurosci.*, vol. 35, fasc. 17, pp. 6667–6688, apr. 2015, doi: 10.1523/JNEUROSCI.4662-14.2015.
[58] N. Mallet *et al.*, «Disrupted Dopamine Transmission and the Emergence of Exaggerated Beta Oscillations in Subthalamic Nucleus and Cerebral Cortex», *J. Neurosci.*, vol. 28, fasc. 18, pp. 4795–4806, apr. 2008, doi: 10.1523/JNEUROSCI.0123-08.2008.
[59] K. J. Mastro, R. S. Bouchard, H. A. K. Holt, e A. H. Gittis, «Transgenic Mouse Lines Subdivide External Segment of the Globus Pallidus (GPe) Neurons and Reveal Distinct GPe Output Pathways», *J. Neurosci.*, vol. 34, fasc. 6, pp. 2087–2099, feb. 2014, doi: 10.1523/JNEUROSCI.4646-13.2014.
[60] K. J. Mastro, K. T. Zitelli, A. M. Willard, K. H. Leblanc, A. V. Kravitz, e A. H. Gittis, «Cell-specific pallidal intervention induces long-lasting motor recovery in dopamine-depleted mice», *Nat. Neurosci.*, vol. 20, fasc. 6, pp. 815–823, giu. 2017, doi: 10.1038/nn.4559.
[61] A. Aristieta e A. Gittis, «Distinct globus pallidus circuits regulate motor and cognitive functions», *Trends Neurosci.*, vol. 44, fasc. 8, pp. 597–599, ago. 2021, doi: 10.1016/j.tins.2021.06.001.
[62] J. Bugaysen, I. Bar-Gad, e A. Korngreen, «Continuous Modulation of Action Potential Firing by a Unitary GABAergic Connection in the Globus Pallidus In Vitro», *J. Neurosci.*, vol. 33, fasc. 31, pp. 12805–12809, lug. 2013, doi: 10.1523/JNEUROSCI.1970-13.2013.
[63] D. J. Hegeman, E. S. Hong, V. M. Hernández, e C. S. Chan, «The external globus pallidus: progress and perspectives», *Eur. J. Neurosci.*, vol. 43, fasc. 10, pp. 1239–1265, mag. 2016, doi: 10.1111/ejn.13196.
[64] N. Mallet *et al.*, «Arkypallidal Cells Send a Stop Signal to Striatum», *Neuron*, vol. 89, fasc. 2, pp. 308–316, gen. 2016, doi: 10.1016/j.neuron.2015.12.017.
[65] J. Lotharius e P. Brundin, «Pathogenesis of parkinson's disease: dopamine, vesicles and α-synuclein», *Nat. Rev. Neurosci.*, vol. 3, fasc. 12, pp. 932–942, dic. 2002, doi: 10.1038/nrn983.

[66] Z. Wei, B.-J. Lin, T.-W. Chen, K. Daie, K. Svoboda, e S. Druckmann, «A comparison of neuronal population dynamics measured with calcium imaging and electrophysiology», *PLOS Comput. Biol.*, vol. 16, fasc. 9, p. e1008198, set. 2020, doi: 10.1371/journal.pcbi.1008198.
[67] J. Magland *et al.*, «SpikeForest, reproducible web-facing ground-truth validation of automated neural spike sorters», *eLife*, vol. 9, p. e55167, mag. 2020, doi: 10.7554/eLife.55167.
[68] A. P. Buccino *et al.*, «SpikeInterface, a unified framework for spike sorting», *eLife*, vol. 9, p. e61834, nov. 2020, doi: 10.7554/eLife.61834.
[69] A. P. Buccino, S. Garcia, e P. Yger, «Spike sorting: new trends and challenges of the era of high-density probes», *Prog. Biomed. Eng.*, vol. 4, fasc. 2, p. 022005, apr. 2022, doi: 10.1088/2516-1091/ac6b96.